A zinc-responsive fluorophore based on 5′-(*p*-hydroxyphenyl)-pyridylthiazole: Electronic Supplementary Information

Yuichiro Watanabe,[1] Wanna Sungnoi,[1] Andrew O. Sartorio,[2] Matthias Zeller,[1] and Alexander Wei[,1,3]*

[1]Department of Chemistry, Purdue University, West Lafayette, IN 47907
[2]Davidson School of Chemical Engineering, Purdue University, West Lafayette, IN 47907
[3]School of Materials Engineering, Purdue University, 701 W. Stadium Avenue, West Lafayette, Indiana 47907, USA.

*E-mail: alexwei@purdue.edu

Table of Contents

1. DFT calculations

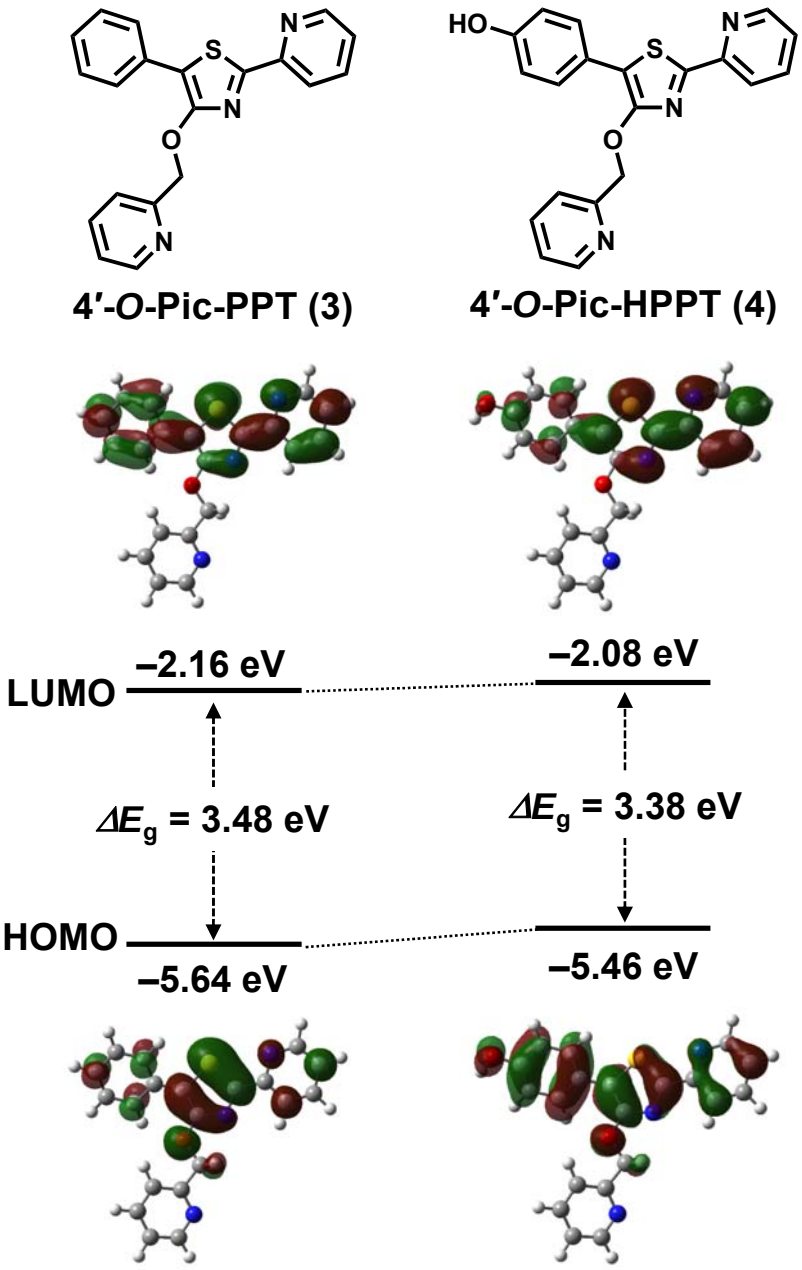

Figure S1. DFT calculations of energy bands and spatial distributions of molecular orbital coefficients (HOMO and LUMO) for 4′-*O*-Pic-PPT (**3**) and 4′-*O*-Pic-HPPT (**4**).

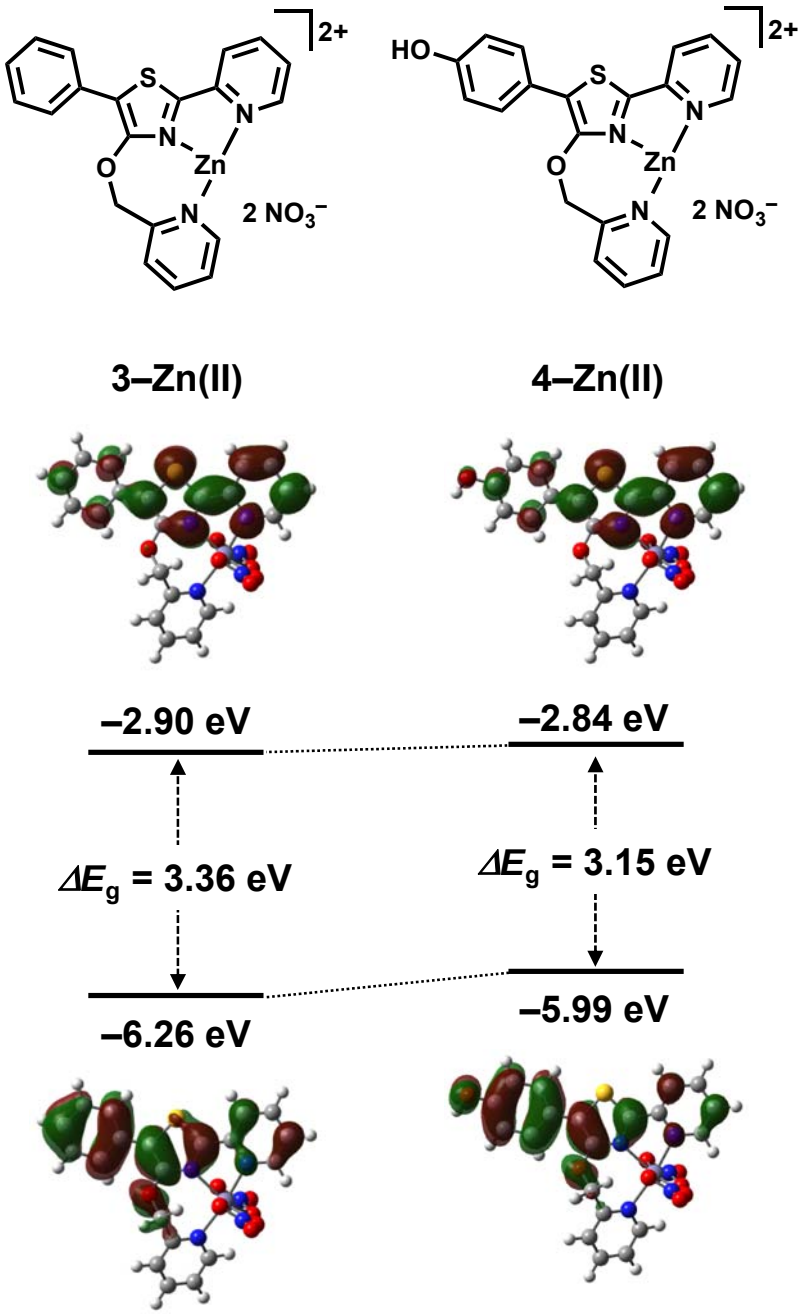

Figure S2. DFT calculations of energy bands and spatial distributions of molecular orbital coefficients (HOMO and LUMO) for **3–Zn(II)** and **4–Zn(II)**.

Table S1. HOMO, LUMO, and ΔE_{H-L} values (eV) for **1–4** and their Zn(II) complexes

Compound	HOMO	LUMO	ΔE_{H-L}[a]
4′-*O*-Et-PPT (**1**)	–5.52	–2.13	3.39
4′-*O*-Et-HPPT (**2**)	–5.32	–2.04	3.28
4′-*O*-Pic-PPT (**3**)	–5.64	–2.16	3.48
4′-*O*-Pic-HPPT (**4**)	–5.46	–2.08	3.38
1–Zn(II)	–6.66	–3.48	3.18
2–Zn(II)	–6.37	–3.42	2.95
3–Zn(II)	–6.26	–2.90	3.36
4–Zn(II)	–5.99	–2.84	3.15

[a] ΔE_{H-L} = LUMO – HOMO.

2. Synthesis

4′-*O*-Et-PPT (**1**) and PPT were synthesized according to previous procedures.[1]

4'-*O*-Et-HPPT (2)

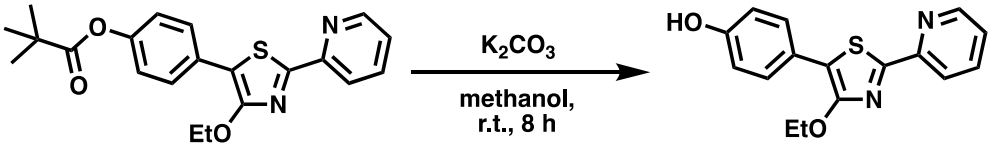

4′-*O*-Et-Piv-PPT (8) | 4′-*O*-Et-HPPT (2)

Compound **8** (233 mg, 0.61 mmol) in methanol (12.5 mL) was treated with K_2CO_3 (253 mg, 1.83 mmol) to produce an initially yellow solution. The reaction mixture was stirred for 8.5 hours at room temperature, during which the solution gradually turned orange then red. The reaction mixture was diluted with water (20 mL) and extracted with dichloromethane (3 × 10 mL). The organic phase was washed with NH_4Cl followed by brine, then dried over Na_2SO_4 and concentrated under reduced pressure to afford **2** as a yellow solid (195 mg, quant.). ^{1}H NMR (300 MHz, acetone-d_6): δ 8.57 (s, 1H), 8.09 (d, J = 7.9 Hz, 1H), 7.90 (t, J = 7.8 Hz, 1H), 7.68 (d, J = 8.1 Hz, 2H), 7.40 (t, J = 6.2 Hz, 1H), 6.90 (d, J = 7.7 Hz, 2H), 4.54 (q, J = 6.8 Hz, 2H), 1.44 (t, J = 6.9 Hz, 3H). ^{13}C NMR (75 MHz, acetone-d_6): δ 160.25, 159.06, 157.68, 152.14, 150.56, 138.19, 129.39, 125.40, 124.14, 119.47, 116.89, 116.69, 115.75, 67.05, 15.96. ESI MS: *m/z* 299 $[M+H]^+$.

4′-*O*-Pic-PPT (**3**)

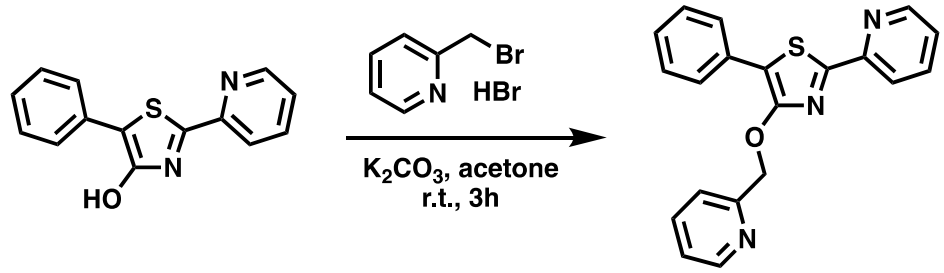

PPT | 4′-*O*-Pic-PPT (3)

A solution of PPT (20 mg, 0.079 mmol) in acetone (4.0 mL) was treated with K_2CO_3 (311 mg, 2.25 mmol) at room temperature to produce a dark red solution. The reaction mixture was then treated with 2-picolyl bromide hydrobromide (PicBr·HBr; 40 mg, 0.160 mmol) and stirred for 12 hours at room temperature. The reaction mixture was diluted with water (10 mL) and extracted with chloroform (3 × 10 mL). The organic phase was washed with NH_4Cl followed by brine, then dried over Na_2SO_4 and concentrated under reduced pressure. The residue was purified by silica gel chromatography using 1% methanol in chloroform (v/v) to afford picolyl ether **3** as a yellow solid (12.8 mg, 58%). ^{1}H NMR (400 MHz, acetone-d_6) δ 8.64–8.57 (m, 2H), 8.12 (dt, J = 7.9, 1.1 Hz, 1H), 7.94 (dt, J = 1.7, 7.8 Hz, 1H), 7.91–7.86 (m, 2H), 7.81 (dt, J = 1.8, 7.7 Hz, 1H), 7.61 (d, J = 7.8 Hz, 1H), 7.49–7.40 (m, 3H), 7.34–7.26 (m, 2H), 5.72 (s, 2H).^{13}C NMR (101 MHz, acetone-d_6) δ 162.83, 159.53, 158.50, 151.83, 150.67, 150.31, 138.33, 137.70, 132.54, 129.89, 128.11, 128.01, 125.82, 123.72, 122.31, 119.73, 73.59. ESI-MS: *m/z* 346 $[M+H]^+$.

4′-*O*-Pic-HPPT (4)

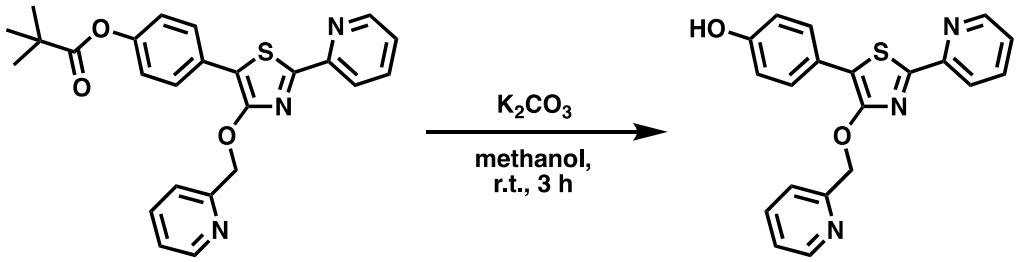

4′-*O*-Pic-Piv-PPT (9) | 4′-*O*-Pic-HPPT (4)

Compound **9** (264 mg, 0.59 mmol) in methanol (20 mL) was treated with K_2CO_3 (245 mg, 1.78 mmol) to produce an initially yellow solution. The reaction mixture was stirred for 3 hours at room temperature, during which the solution gradually turned orange then red. The reaction mixture was diluted with water (25 mL) and extracted with dichloromethane (3 × 50 mL). The organic phase was washed with NH_4Cl followed by brine, then dried over Na_2SO_4 and concentrated under reduced pressure. The residue was purified by silica gel chromatography using gradient elution with 0–5% methanol in chloroform (v/v) to afford Pic-HPPT **4** as a yellow solid (214 mg, quant.). ^{1}H NMR (800 MHz, acetone-d_6): δ 8.65–8.55 (m, 3H), 8.08 (d, J = 7.9 Hz, 1H), 7.91 (t, J = 7.6 Hz, 1H), 7.80 (t, J = 7.6 Hz, 1H), 7.73 (d, J = 8.7 Hz, 2H), 7.59 (d, J = 7.9 Hz, 1H), 7.41 (m, 1H), 7.30 (m, 1H), 6.92 (d, J = 8.6 Hz, 2H), 5.68 (s, 2H). ^{13}C NMR (201 MHz, acetone-d_6) δ 160.54, 158.65, 158.43, 157.92, 152.01, 150.58, 150.25, 138.22, 137.66, 129.58, 125.47, 123.79, 123.64, 122.24, 119.51, 116.77, 116.25, 73.46. ESI-MS: *m/z* 362 $[M+H]^+$.

4-(2'-Ethoxy-2'-oxoethyl)phenyl pivalate (5)

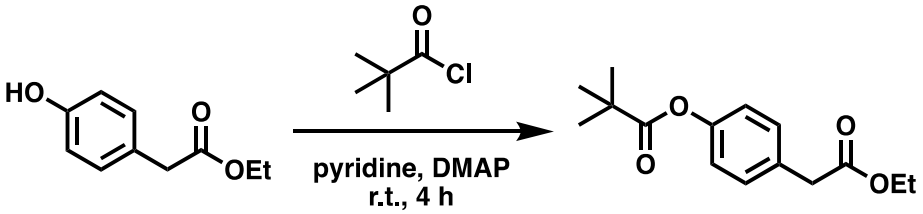

5

A mixture of ethyl 4-hydroxyphenylacetate (2.01 g, 11.2 mmol) and pyridine (50 mL) were degassed with argon for 5 minutes, then treated with pivaloyl chloride (PivCl; 4.05 g, 33.6 mmol) and 4-dimethylaminopyridine (DMAP; 55 mg, 0.45 mmol) and stirred for 4 hours at room temperature. The mixture was concentrated under reduced pressure, and the residue was purified by silica gel chromatography using 5% ethyl acetate in hexane (v/v) to afford pivalate **5** as a colorless oil (3.34 g, quant.). ^{1}H NMR (400 MHz, $CDCl_3$): δ 7.29 (d, J = 8.7 Hz, 2H), 7.01 (d, J = 8.5 Hz, 2H), 4.14 (q, J = 7.1 Hz, 2H), 3.59 (s, 2H), 1.35 (s, 9H), 1.24 (t, J = 7.1 Hz, 3H). ^{13}C NMR (101 MHz, $CDCl_3$): δ 177.31, 171.64, 150.45, 131.73, 130.48, 121.83, 61.20, 41.11, 39.36, 27.43, 14.46. ESI-MS: *m/z* 287 $[M+Na]^+$.

4-(1'-Bromo-2'-ethoxy-2'-oxoethyl)phenyl pivalate (6)

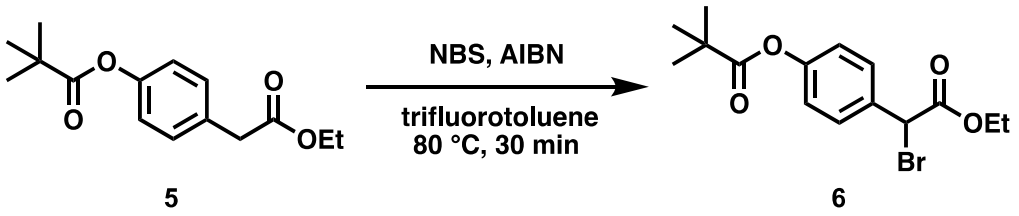

5 6

Compound **4** (3.965 g, 15.0 mmol) and *N*-bromosuccinimide (NBS; 2.937 g, 16.5 mmol)) were added to a 50-mL round-bottomed flask and dissolved in α,α,α-trifluorotoluene (TFT; 21.5 mL), then degassed with argon for 5 min. Azobisisobutyronitrile (AIBN; 246 mg, 1.50 mmol) was added to the reaction mixture, which was heated to 80 °C under argon and stirred for 30 min. The mixture was cooled to room temperature, diluted with 50 mL of hexanes, then subjected directly to silica gel chromatography using 2.5% ethyl acetate in hexanes (v/v). α-Bromoester **6** was isolated as a yellow oil (3.92 g, 76% yield). ^{1}H NMR (400 MHz, $CDCl_3$): δ 7.56 (d, J = 8.7 Hz, 2H), 7.06 (d, J = 8.6 Hz, 2H), 5.33 (s, 1H), 4.29–4.14 (m, 2H), 1.34 (s, 9H), 1.26 (t, J = 7.1 Hz, 3H). ^{13}C NMR (101 MHz, $CDCl_3$): δ 176.67, 168.08, 151.63, 133.07, 129.84, 121.85, 62.53, 46.02, 39.08, 27.06, 13.89. ESI-MS: *m/z* 323 $[M+H]^+$.

4-(4'-Hydroxy-2'-(pyridin-2"-yl)thiazol-5'-yl)phenyl pivalate (7)

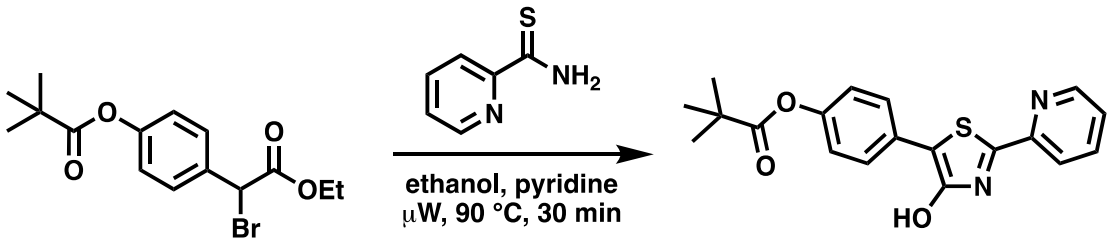

6 Piv-PPT (7)

A mixture of compound **6** (1.72 g, 5.00 mmol), 2-pyridylthioamide (0.658 g, 4.76 mmol), pyridine (115 μL, 1.43 mmol), and ethanol (1 mL) were degassed with argon for 5 min in a microwave (μW) reaction tube. The reaction mixture was subjected to microwave heating at 90 °C (45 W) under argon for 30 min, then cooled to room temperature. Yellow crystals were precipitated and collected, then washed with cold ethanol to afford a batch of 4'-hydroxythiazole **7**. The liquid residue was concentrated to dryness, then redissolved and recrystallized in cold ethanol (20 mL). The total weight of crystalline **7** was 549 mg (33% yield). ^{1}H NMR (300 MHz, acetone-d_6): δ 10.27 (s, 1H), 8.59 (br. d, J = 4.4 Hz, 1H), 8.02 (dt, J = 8.0, 1.1 Hz, 1H), 7.96–7.83 (m, 3H), 7.43 (ddd, J = 1.3, 4.8, 7.5 Hz, 1H), 7.17 (d, J = 8.8 Hz, 2H), 1.36 (s, 9H). ^{13}C NMR (75 MHz, acetone-d_6): δ 177.26, 162.07, 159.83, 151.84, 150.90, 150.69, 138.32, 130.76, 128.45, 125.77, 123.16, 119.58, 111.68, 40.00, 27.75. ESI-MS: *m/z* 355 $[M+H]^+$.

4-(4'-Ethoxy-2'-(pyridin-2"-yl)thiazol-5'-yl)phenyl pivalate (8)

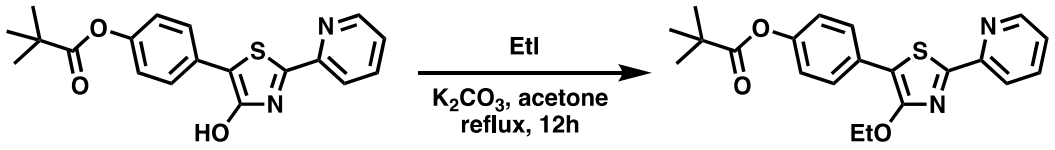

Piv-PPT (7) 4′-*O*-Et-Piv-PPT (8)

Compound **7** (242 mg, 0.68 mmol) in acetone (35 mL) was treated with K_2CO_3 (61 mg, 0.75 mmol) at room temperature to produce a dark red solution. The reaction mixture was treated with iodoethane (EtI; 0.55 mL, 6.83 mmol), heated to reflux, and stirred for 12 hours. The reaction mixture was diluted with water (20 mL) and extracted with dichloromethane (3 × 40 mL). The organic phase was washed with NH_4Cl followed by brine, then dried over Na_2SO_4 and concentrated under reduced pressure. The residue was purified by silica gel chromatography using dichloromethane to afford ethyl ether **8** as a yellow solid (245 mg, 94%). ^{1}H NMR (300 MHz, acetone-d_6): δ 8.60 (br. d, J = 4.4 Hz, 1H), 8.13 (d, J = 7.9 Hz, 1H), 7.94 (dt, J = 7.8, 1.7 Hz, 1H), 7.86 (d, J = 8.7 Hz, 2H), 7.47 (ddd, J = 1.3, 5.2, 7.1 Hz, 1H), 7.17 (d, J = 8.7 Hz, 2H), 4.59 (q, J = 7.0 Hz, 2H), 1.47 (t, J = 7.0 Hz, 3H), 1.35 (s, 9H). ^{13}C NMR (75 MHz, acetone-d_6): δ 177.28, 162.04, 160.13, 151.94, 151.18, 150.71, 138.37, 130.34, 128.81, 125.85, 123.22, 119.74, 114.22, 67.35, 40.03, 27.76, 15.97. ESI-MS: *m/z* 383 $[M+H]^+$.

4-(4'-(2"-pyridyl)methoxy-2'-(pyridin-2"-yl)thiazol-5'-yl)phenyl pivalate (9)

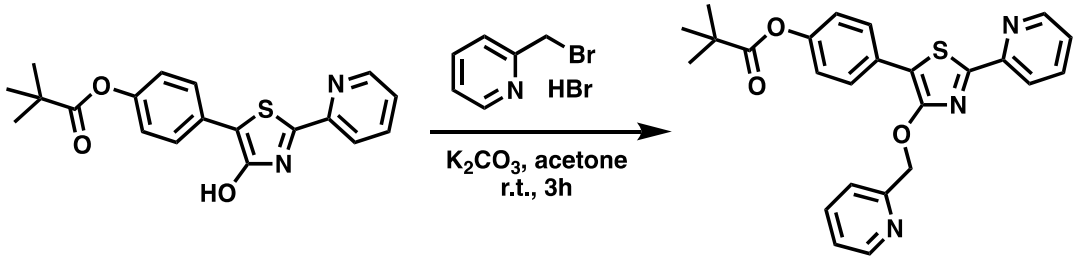

Piv-PPT (7) 4′-*O*-Pic-Piv-PPT (9)

Compound **7** (351 mg, 0.99 mmol) in acetone (50 mL) was treated with K_2CO_3 (2.74 g, 19.8 mmol) at room temperature to produce a dark red solution. The reaction mixture was treated with PicBr·HBr (502 mg, 1.98 mmol) and stirred for 3 hours at room temperature, during which the red solution turned a pale pink. The reaction mixture was diluted with water (20 mL) and extracted with chloroform (3 × 50 mL). The organic phase was washed with NH_4Cl followed by brine, then dried over Na_2SO_4 and concentrated under reduced pressure. The residue was purified by silica gel column chromatography using 20% ethyl acetate in hexanes (v/v) to afford picolyl ether **9** as a yellow solid (348 mg, 79%). ^{1}H NMR (400 MHz, acetone-d_6) δ 8.56 (m, 2H), 8.08 (dt, J = 1.1, 7.9 Hz, 1H), 7.94–7.85 (m, 3H), 7.78 (dt, J = 1.8, 7.7 Hz, 1H), 7.58 (d, J = 7.9 Hz, 1H), 7.41 (ddd, J = 1.2, 4.8, 7.5 Hz, 1H), 7.27 (dd, J = 4.8, 7.9 Hz, 1H), 7.15 (d, J = 8.9 Hz, 2H), 5.68 (s, 2H), 1.32 (s, 9H). ^{13}C NMR (101 MHz, acetone-d_6): δ 177.25, 162.21, 159.42, 158.38, 151.73, 151.31, 150.65, 150.29, 138.33, 137.70, 129.94, 128.91, 125.84, 123.70, 123.20, 122.29, 119.70, 114.45, 73.59, 39.77, 27.47. ESI MS: *m/z* 446 $[M+H]^+$.

3. Single-crystal X-ray crystallography

Single-crystal X-ray diffraction studies were carried out in the Purdue X-Ray Crystallography Facility using a Bruker AXS D8 Quest CMOS diffractometer. A single crystal of **4'-*O*-Pic-HPPT (4)** was grown by slow solvent evaporation in acetone at room temperature. A single crystal of **4–Zn(II)** nitrate was grown by slow solvent evaporation in CH_3CN at room temperature. Yellow crystals suitable for X-ray analysis were selected for intensity measurements. Single crystals were coated with fomblin (Solvay) oil then quickly transferred to the goniometer head of the Bruker Quest diffractomerter. Diffraction and data collection were performed with Mo *K*α radiation (λ = 0.71073 Å) at 150 K. All crystal data and structure refinements are listed in Table S2–S3. Data were collected, reflections were indexed and processed, and the files scaled and corrected for absorption using APEX3.[2] Space group assignments and structures were solved by direct methods using XPREP within the SHELXTL suite of programs,[3] and refined by full matrix least squares against F^2 with all reflections using Shelxl2018,[4,5] using the graphical interface Shelxle.[6] H atoms attached to C and O atoms were positioned geometrically and constrained to ride on their parent atoms, with C–H bond distances of 0.95 Å for aromatic methines and 0.99 Å for the aliphatic methylene, respectively. The C–O–H bond angle was kept fixed but the O–H distance and torsion angle were refined according to the best fit to the experimental electron density (AFIX 148). U_{iso}(H) values were set to a multiple of U_{eq}(O/C) with 1.5 for OH units and 1.2 for CH and CH_2 units, respectively.

Crystals of **4–Zn(II)** were found to be non-merohedrally twinned. The orientation matrices for the two components were identified using the program Cell_Now, with the two components being related by a 180° rotation around the real *c*-axis. The two components were integrated using Saint and corrected for absorption using twinabs, resulting in the following statistics:

21435 data (5819 unique) involve domain 1 only, mean I/sigma 9.8
21483 data (5779 unique) involve domain 2 only, mean I/sigma 4.3
2608 data (1789 unique) involve 2 domains, mean I/sigma 11.9

The exact twin matrix identified by the integration program was found to be:

–1.00698 0.02706 –0.67310
–0.05312 –0.99897 –0.06648
0.02239 –0.02087 1.00701

The structure was solved using direct methods with only the non-overlapping reflections of component 1. The structure was refined using the hklf 5 routine with all reflections of component 1 (including the overlapping ones), resulting in a BASF value of 0.236(4).

The R_{int} value given is for all reflections and is based on agreement between observed single and composite intensities and those calculated from refined unique intensities and twin fractions (TWINABS (Sheldrick, 2012)).

Complete crystallographic data has been deposited in CIF format with the Cambridge Crystallographic Data Centre. CCDC 1960137–1960138 contains the supplementary crystallographic data for this paper. These data can be obtained free of charge from The Cambridge Crystallographic Data Centre via www.ccdc.cam.ac.uk/data_request/cif.

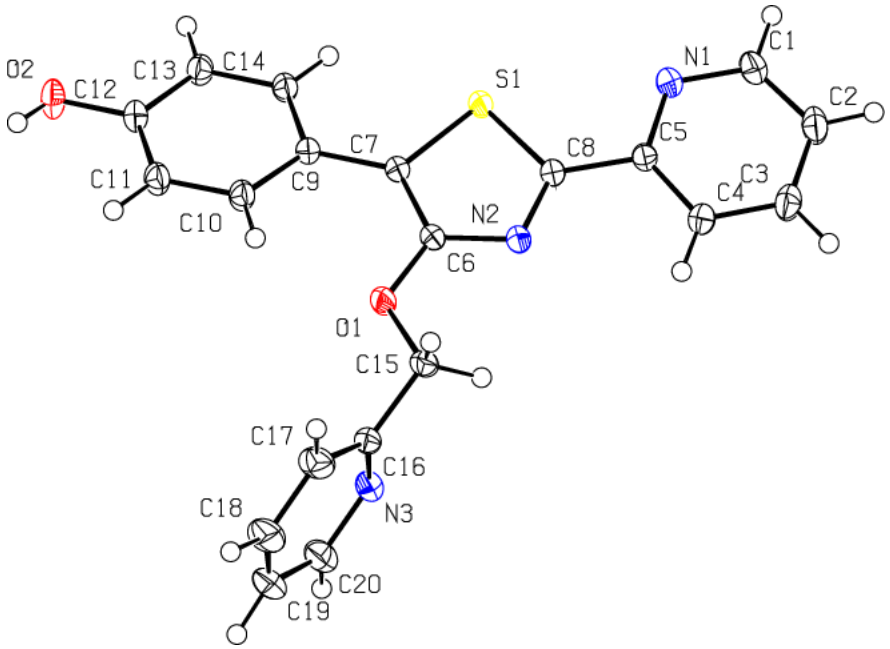

Figure S3. ORTEP diagram of 4′-*O*-Pic-HPPT (**4**) with thermal ellipsoids at 50% probability.

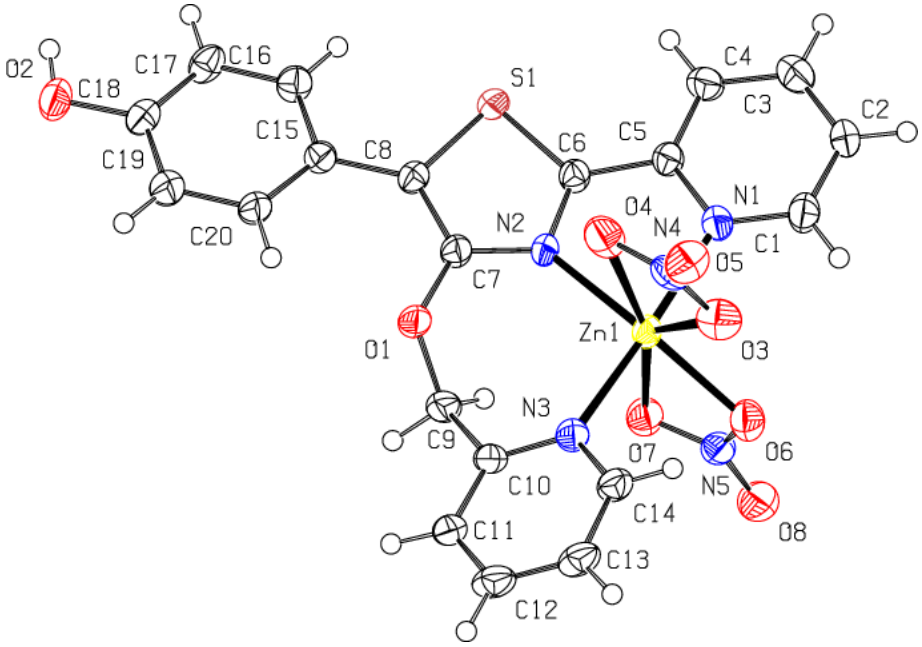

Figure S4. ORTEP diagram of **4–Zn(II)** with thermal ellipsoids at 50% probability.

Table S2. Crystal data and structure refinement for 4'-*O*-Pic-HPPT (**4**)

Crystal data	
Chemical formula	$C_{20}H_{15}N_3O_2S$
*M*r	361.41
Crystal system, space group	Monoclinic, *C*2/c
Temperature (K)	150
a, *b*, *c* (Å)	13.5888 (10), 9.7577 (7), 26.7297 (19)
β (°)	94.128 (2)
V (Å^3)	3535.0 (4)
Z	8
Radiation type	Mo $K\alpha$
μ (mm^{-1})	0.20
Crystal size (mm^3)	0.55 × 0.55 × 0.13
Data collection	
Diffractometer	Bruker AXS D8 Quest CMOS diffractometer
Absorption correction	Multi-scan SADABS 2016/2 [7]
T_{min}, T_{max}	0.667, 0.747
No. of measured, independent and observed [$I > 2\sigma(I)$] reflections	28987, 6732, 5712
R_{int}	0.024
$(\sin \theta/\lambda)_{max}$ ranges (Å^{-1})	0.770
Refinement	
R [$F^2 > 2\sigma(F^2)$], $wR(F^2)$, S	0.038, 0.108, 1.07
No. of reflections	6732
No. of parameters	237
H-atom treatment	H atoms treated by a mixture of independent and constrained refinement
$\Delta\rho_{max}$, $\Delta\rho_{min}$ (e Å^{-3})	0.43, –0.43

Computer programs: Apex3 v2018.1-0 (Bruker, 2018), *SAINT* V8.38A (Bruker, 2016), *SHELXS97* (Sheldrick, 2008), *SHELXL2018*/3 (Sheldrick, 2018), SHELXLE Rev946 (Hübschle *et al.*, 2011).

Table S3. Crystal data and structure refinement for **4–Zn(II)**.

Crystal data	
Chemical formula	$C_{20}H_{15}N_5O_8SZn$
*M*r	550.80
Crystal system, space group	Monoclinic, *C*2/c
Temperature (K)	150
a, *b*, *c* (Å)	14.504 (2), 22.056 (4), 14.355 (2)
β (°)	110.036 (5)
V (Å^3)	4314.1 (12)
Z	8
Radiation type	Mo $K\alpha$
μ (mm^{-1})	1.20
Crystal size (mm^3)	0.19 × 0.06 × 0.05
Data collection	
Diffractometer	Bruker AXS D8 Quest CMOS diffractometer
Absorption correction	Multi-scan TWINABS 2012/1 [7]
T_{min}, T_{max}	0.357, 0.433
No. of measured, independent and observed [$I > 2\sigma(I)$] reflections	8166, 6296, 5042
R_{int}	0.098
$(\sin \theta/\lambda)_{max}$ ranges (Å^{-1})	0.714
Refinement	
R [$F^2 > 2\sigma(F^2)$], $wR(F^2)$, S	0.088, 0.241, 1.12
No. of reflections	6296
No. of parameters	318
H-atom treatment	H atom parameters constrained
$\Delta\rho_{max}$, $\Delta\rho_{min}$ (e Å^{-3})	2.97, –0.58

Computer programs: Apex3 v2018.1-0 (Bruker, 2018), *SAINT* V8.38A (Bruker, 2016), *SHELXS97* (Sheldrick, 2008), *SHELXL2018*/3 (Sheldrick, 2018), SHELXLE Rev946 (Hübschle *et al.*, 2011).

4. Photophysical properties

I. Solvatochromism studies

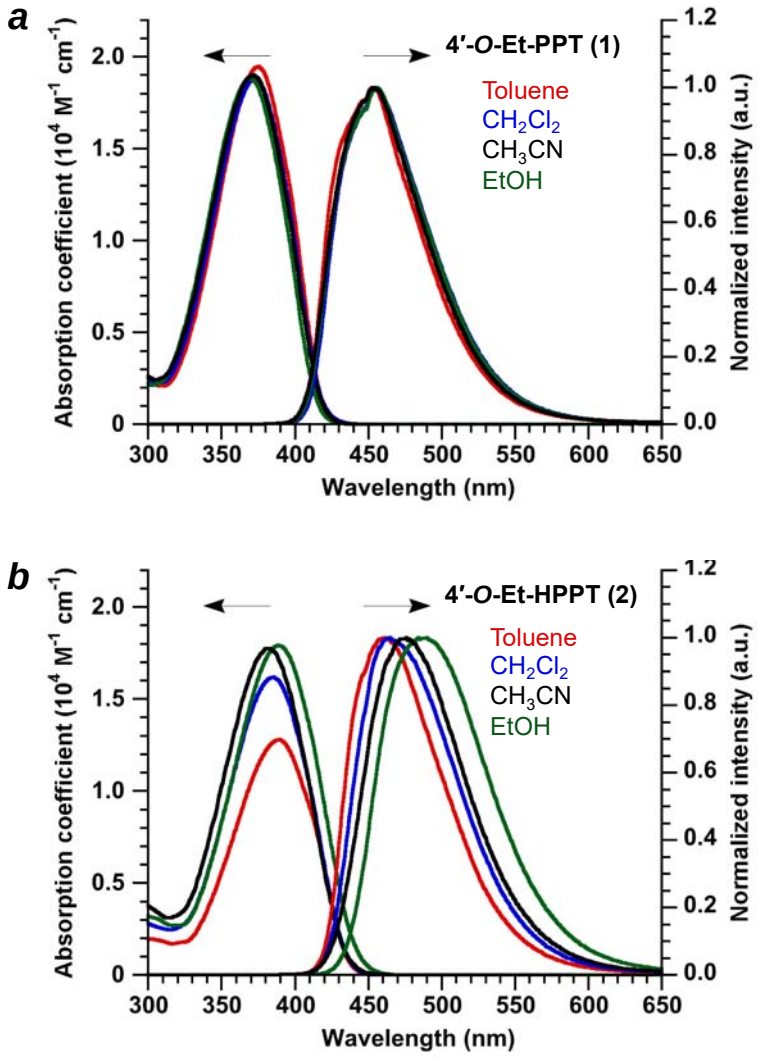

Figure S5. (a) Optical absorption and normalized photoluminescence (PL) spectra of 4′-*O*-Et-PPT (**1**) and (b) 4′-*O*-Et-HPPT (**2**). These spectra were recorded at 30 μM and 20 °C.

Table S4. Photophysical properties of **1–4** in various solvents.

	λ^{max}_{abs} [nm]	λ^{max}_{em} [nm]	ε_{abs} [$\times 10^4$ M^{-1} cm^{-1}]	ν_{St} [cm^{-1}] / nm
4'-*O*-Et-PPT (**1**)				
Toluene	375	453	1.95	4592 / 78
CH_2Cl_2	373	456	1.88	4880 / 83
CH_3CN	371	454	1.90	4928 / 83
EtOH	369	456	1.88	5170 / 87
4'-*O*-Et-HPPT (**2**)				
Toluene	389	461	1.28	4015 / 72
CH_2Cl_2	386	465	1.62	4401 / 79
CH_3CN	383	476	1.77	5101 / 93
EtOH	388	487	1.79	5239 / 99
4'-*O*-Pic-PPT (**3**)				
Toluene	375	451	1.95	4494/ 76
CH_2Cl_2	373	453	1.88	4735/ 80
CH_3CN	369	454	1.97	5074/ 85
EtOH	369	454	1.88	5074/ 85
4'-*O*-Pic-HPPT (**4**)				
Toluene	384	457	1.69	4160 / 73
CH_2Cl_2	381	462	1.78	4602 / 81
CH_3CN	380	472	2.07	5129 / 92
EtOH	384	486	1.86	5466 / 102

II. Quantum yield analysis

The photoluminescence quantum yield (Φ_{PL}) is the ratio of the number of photons emitted (N^{em}) to the number of photons absorbed (N^{abs}). Spectral scans of the excitation scatter region (S_{ref} and S_{sample}) and the emission regions of the sample and solvent (E_{sample} and E_{ref}) were used to calculate PL quantum yields, according to Equation S1:

$$\Phi_{PL} = \frac{N^{em}}{N^{abs}} = \frac{E_{sample} - E_{ref.}}{S_{ref.} - S_{sample}} \qquad \text{(S1)}$$

All samples were dissolved in CH_3CN (30 μM) and degassed with N_2 for 1 min. Excitation wavelength bandwidth ($\Delta\lambda_{ex}$) is 6 nm; emission wavelength bandwidth ($\Delta\lambda_{em}$) is 0.15 nm.

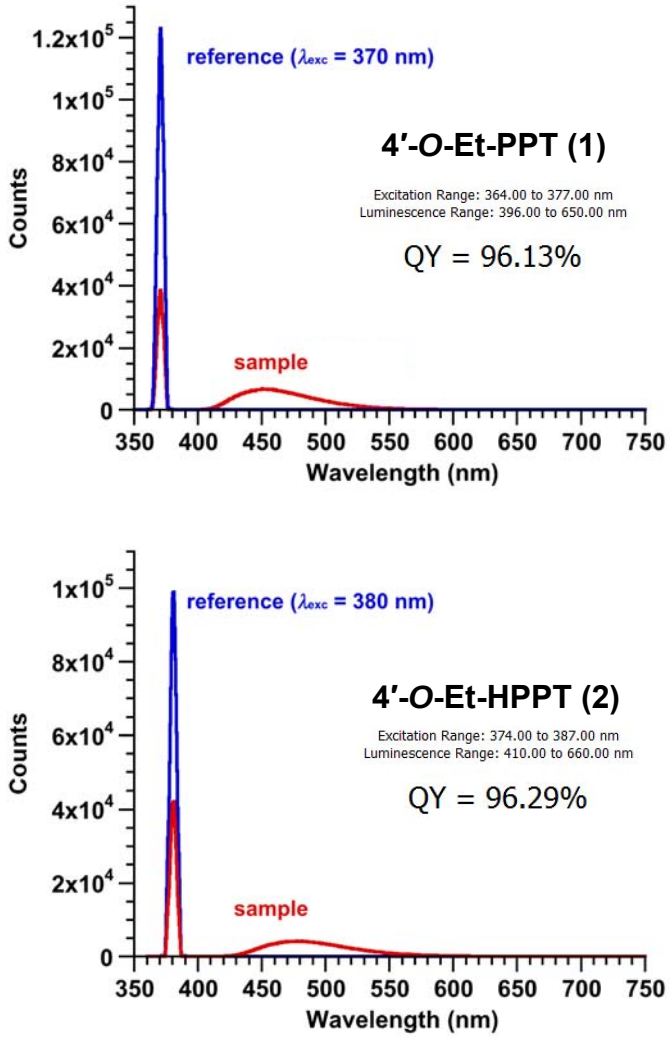

Figure S6. Spectral scans of the excitation scatter region (reference) and the emission regions of the sample (4'-*O*-Et-PPT (**1**) and 4'-*O*-Et-HPPT (**2**)) and solvent to calculate PL quantum yields.

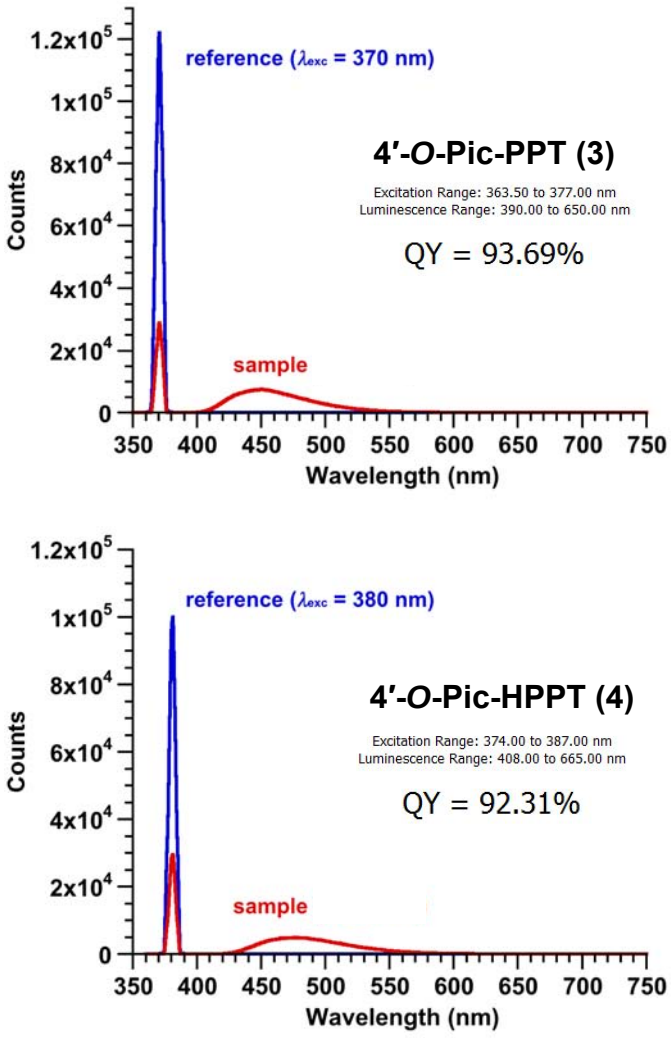

Figure S7. Spectral scans of the excitation scatter region (reference) and the emission region of the sample (4'-*O*-Pic-PPT (**3**) and 4'-*O*-Pic-HPPT (**4**)) and the solvent to calculate PL quantum yields.

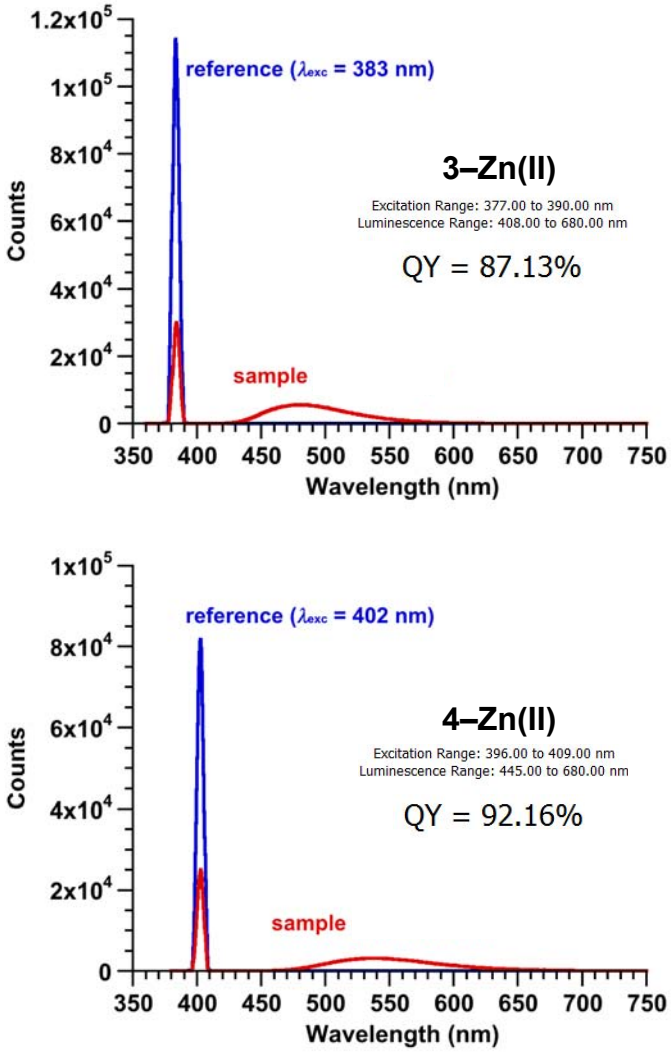

Figure S8. Spectral scans of the excitation scatter region (reference) and the emission region of the sample (**3–Zn(II)** and **4–Zn(II)**) and the solvent to calculate PL quantum yields.

III. Commission Internationale de L'Eclairage (CIE) chromaticity coordinates

CIE 1931 colour space chromaticity coordinates were analysed with Edinburgh instruments FLS 980 software. All perceived colours can be translated into differing amounts of the three primary colours corresponding to the photoreceptors of the human eye (cone cell sensitivity). Different levels of stimulus to the amount of each primary colour gives rise to three parameters (tristimulus values *X*, *Y*, and *Z*) that can describe any perceived colour, as quantified by Equations S2–S4:

$$X = \int_0^\infty I(\lambda)\bar{x}(\lambda)d\lambda \qquad \text{(S2)}$$

$$Y = \int_0^\infty I(\lambda)\bar{y}(\lambda)d\lambda \qquad \text{(S3)}$$

$$Z = \int_0^\infty I(\lambda)\bar{z}(\lambda)d\lambda \qquad \text{(S4)}$$

The calculation of CIE 1931 coordinates (*x*,*y*) are based on Equations S5 and S6:

$$x = \frac{X}{X+Y+Z} \qquad \text{(S5)}$$

$$y = \frac{Y}{X+Y+Z} \qquad \text{(S6)}$$

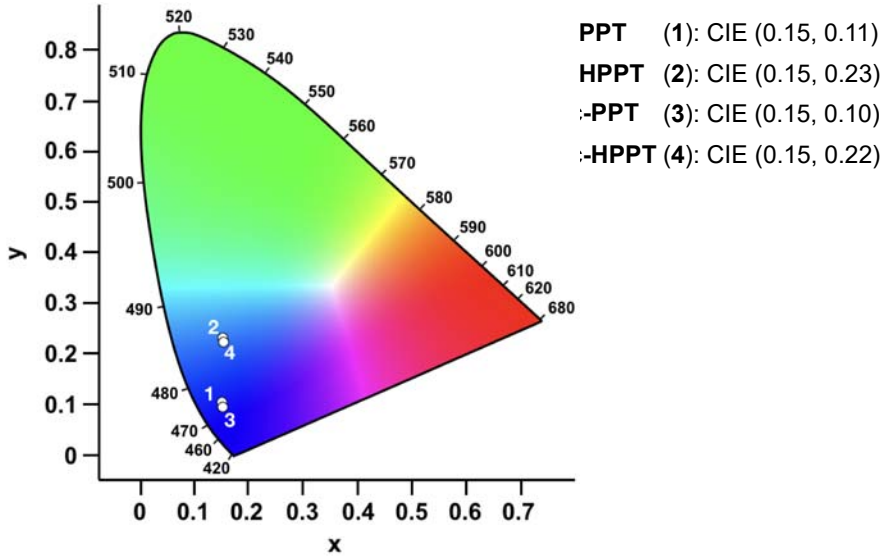

Figure S9. CIE chromaticity diagram for **1–4** in CH_3CN solution (30 μM).

Table S5. CIE coordinates corresponding to titration of $Zn(NO_3)_2$ to 4'-*O*-Pic-PPT (**3**)

Equiv. of Zn(II)	*x*	*y*
0	0.15	0.10
0.1	0.15	0.11
0.2	0.15	0.13
0.3	0.15	0.14
0.4	0.15	0.16
0.5	0.15	0.18
0.6	0.15	0.20
0.7	0.15	0.22
0.8	0.15	0.24
0.9	0.15	0.25
1	0.16	0.25

Table S6. CIE coordinates corresponding to titration of $Zn(NO_3)_2$ to 4'-*O*-Pic-HPPT (**4**).

Equiv. of Zn(II)	*x*	*y*
0	0.15	0.22
0.1	0.16	0.23
0.2	0.18	0.27
0.3	0.20	0.31
0.4	0.23	0.36
0.5	0.25	0.40
0.6	0.28	0.45
0.7	0.30	0.49
0.8	0.32	0.53
0.9	0.34	0.56
1	0.34	0.56

IV. Titration of Zn^{2+} to PPT derivatives in CH_3CN

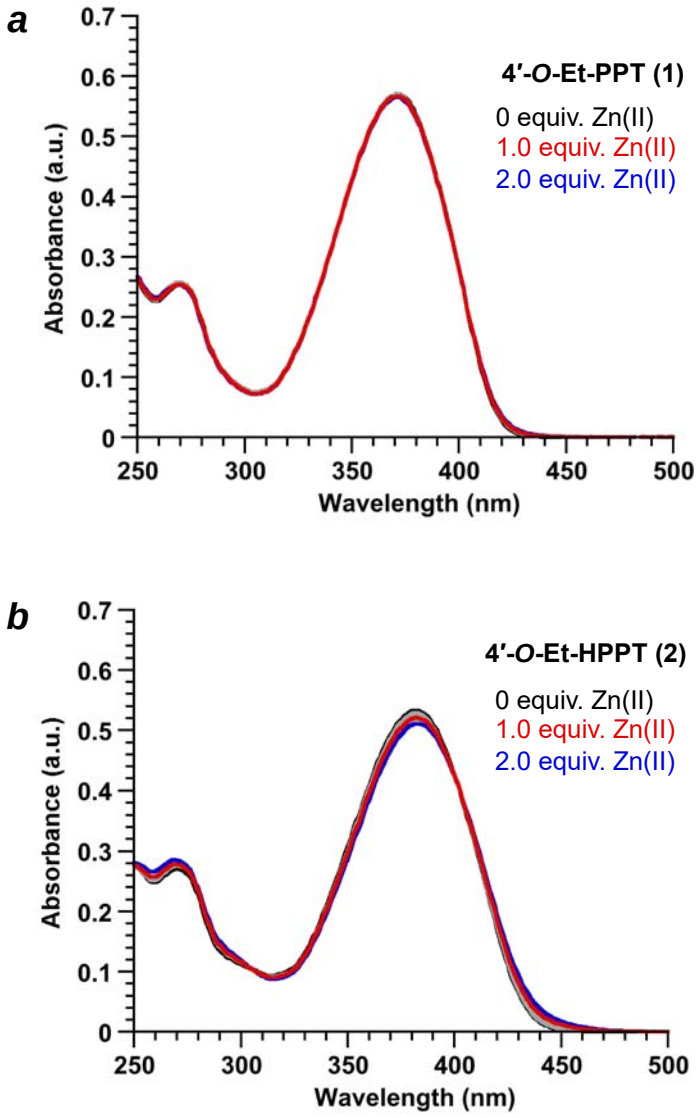

Figure S10. (a) UV–vis absorption spectra for titration study by adding $Zn(NO_3)_2 \cdot 6\ H_2O$ (3 mM in CH_3CN) to 4′-*O*-Et-PPT (**1**). (b) UV–vis absorption spectra for titration study to 4′-*O*-Et-HPPT (**2**). Spectra were recorded at 30 μM and 20 °C in CH_3CN.

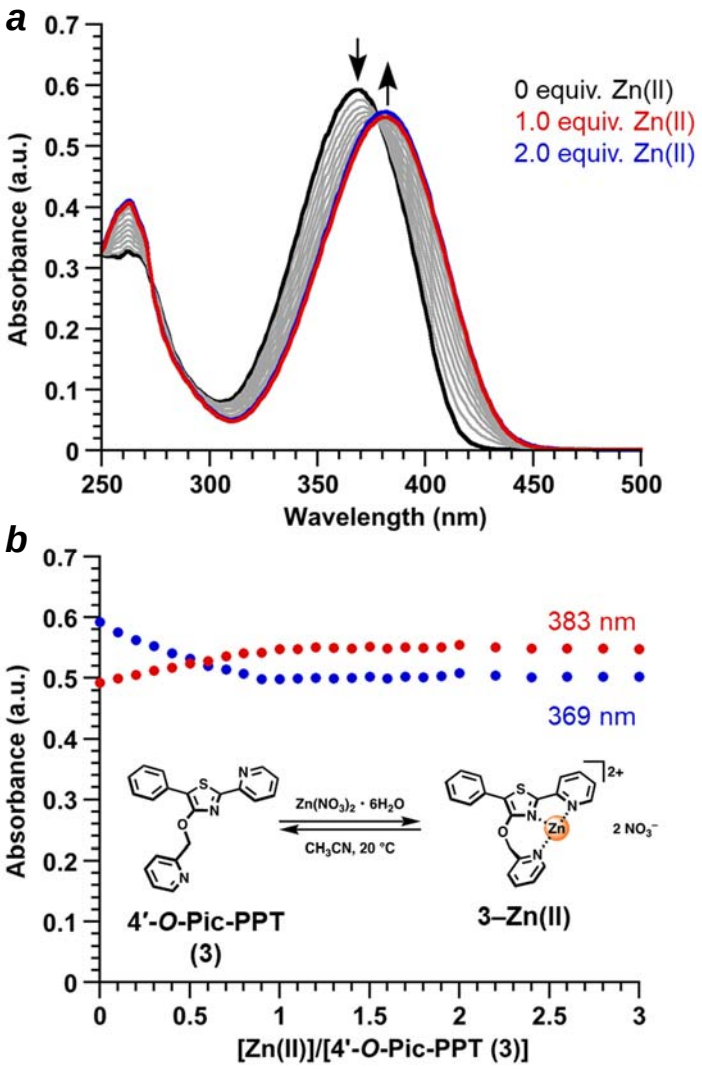

Figure S11. (a) Spectral changes in the absorbance of **3** (30 μM in CH_3CN) upon titration of $Zn(NO_3)_2 \cdot 6\ H_2O$ (3 mM in CH_3CN). (b) Stoichiometry of **3–Zn(II)** complex formation in CH_3CN using the molar ratio method, based on absorbance maxima.

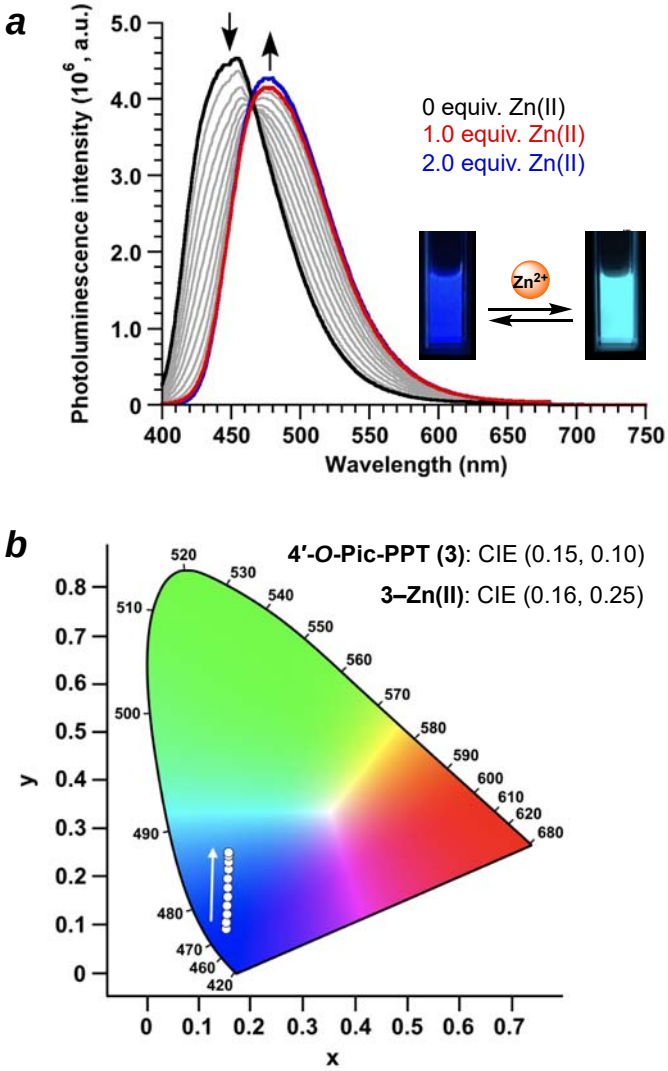

Figure S12. (a) Photoluminescence (PL) spectra corresponding to titration of $Zn(NO_3)_2 \cdot 6\ H_2O$ to 4'-*O*-Pic-PPT (**3**), with excitation at 377 nm (isosbestic point). (b) CIE chromaticity diagram of **3** during $Zn(NO_3)_2$ titration, up to one molar equivalent.

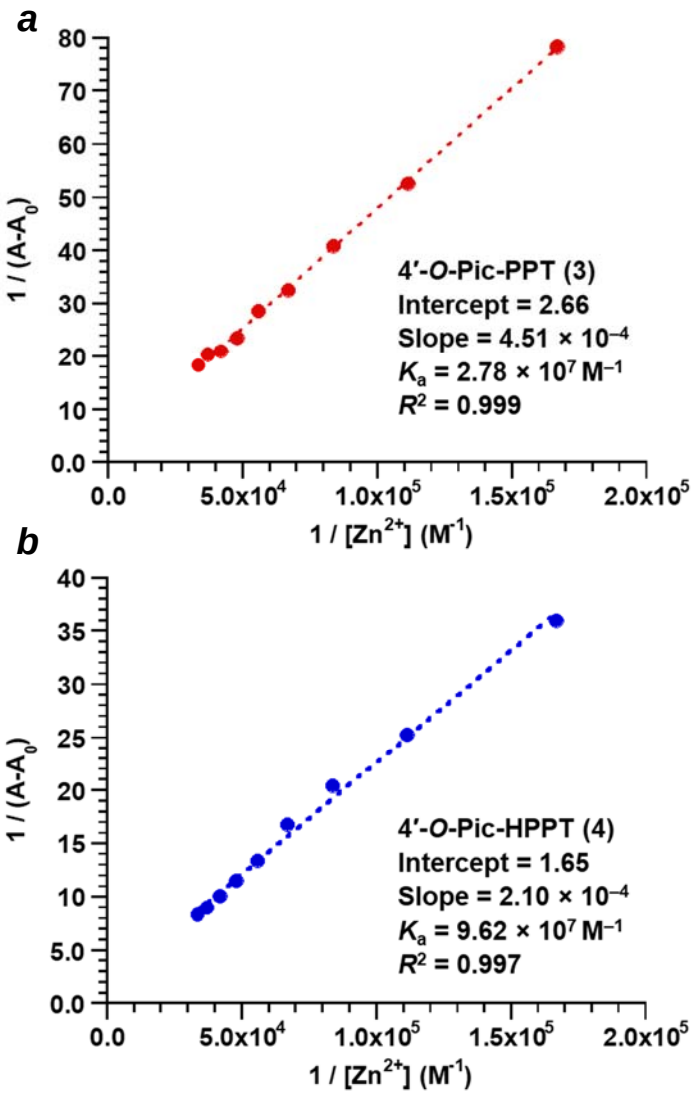

Figure S13. Association constants (K_a values) for PPT derivatives **3** and **4** (30 μM in CH_3CN) and Zn^{2+} ion, determined by UV–vis absorption using the Benesi–Hildebrand method. [8] (a) Double reciprocal plot for **3** ($1/(A–A_0)$ vs. $1/[Zn^{2+}]$), based on λ_{max} of **3–Zn(II)** (383 nm); (b) double reciprocal plot for **4**, based on λ_{max} of **4–Zn(II)** (402 nm). $A–A_0$ is the change in absorbance with incremental Zn^{2+} addition.

V. Counterion effects in Zn(II) complexation

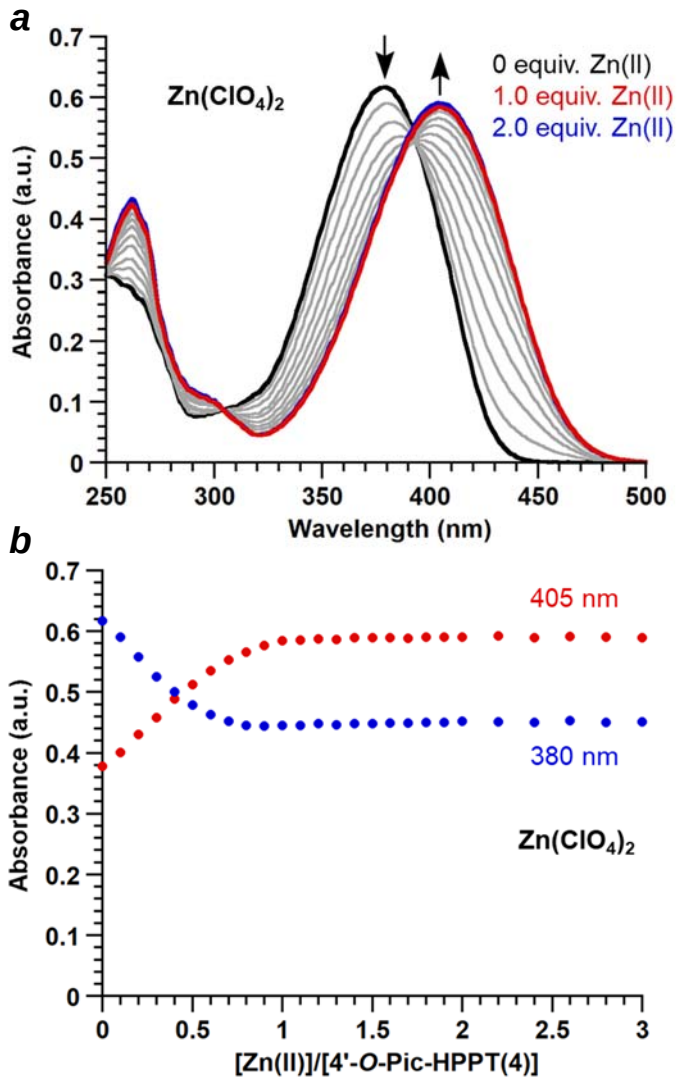

Figure S14. (a) Spectral changes in the absorbance of 4'-*O*-Pic-HPPT **4** (30 μM in CH_3CN) upon titration of $Zn(ClO_4)_2 \cdot 6\ H_2O$ (3 mM in CH_3CN). (b) Stoichiometry of **4–Zn(II)** complex formation in CH_3CN using the molar ratio method, based on absorbance maxima.

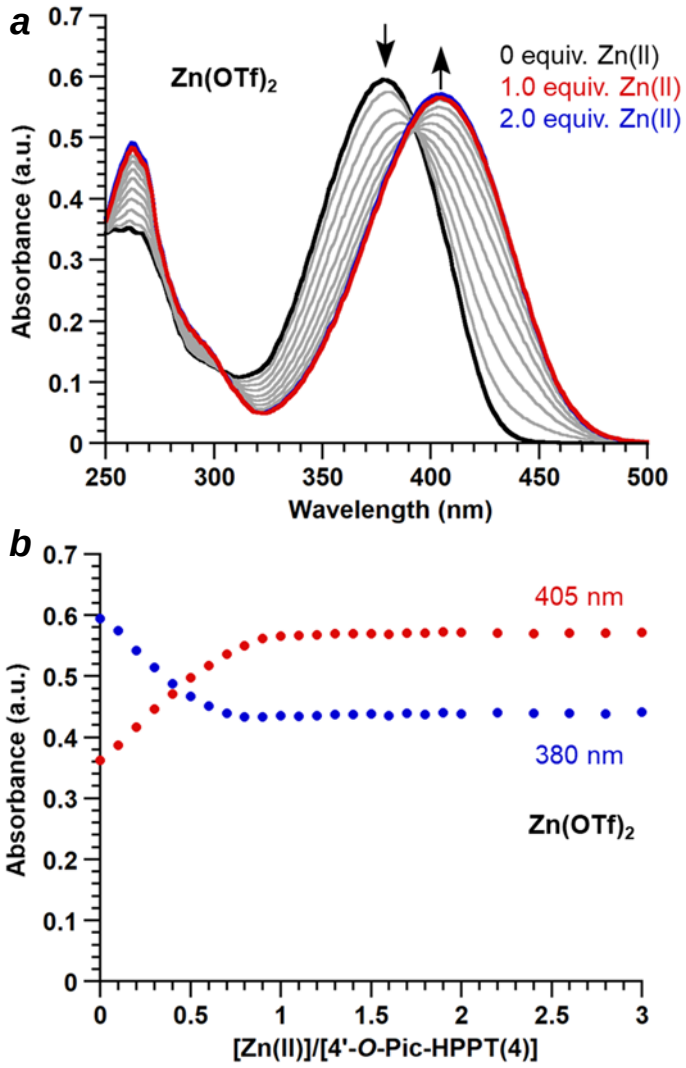

Figure S15. (a) Spectral changes in the absorbance of 4'-*O*-Pic-HPPT **4** (30 μM in CH_3CN) upon titration of $Zn(OTf)_2$ (3 mM in CH_3CN). (b) Stoichiometry of **4–Zn(II)** complex formation in CH_3CN using the molar ratio method, based on absorbance maxima.

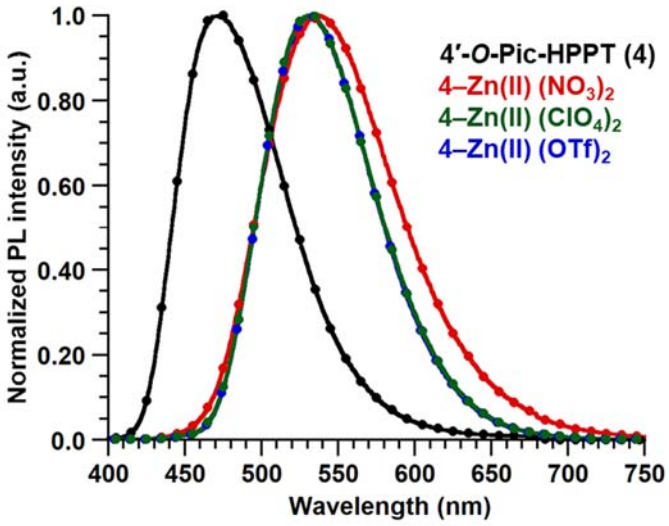

Figure S16. PL spectra of **4** and **4–Zn(II)** complexes with various counterions (λ_{ex} = 393 nm).

VI. Stokes shifts of PPT–Zn(II) complexes

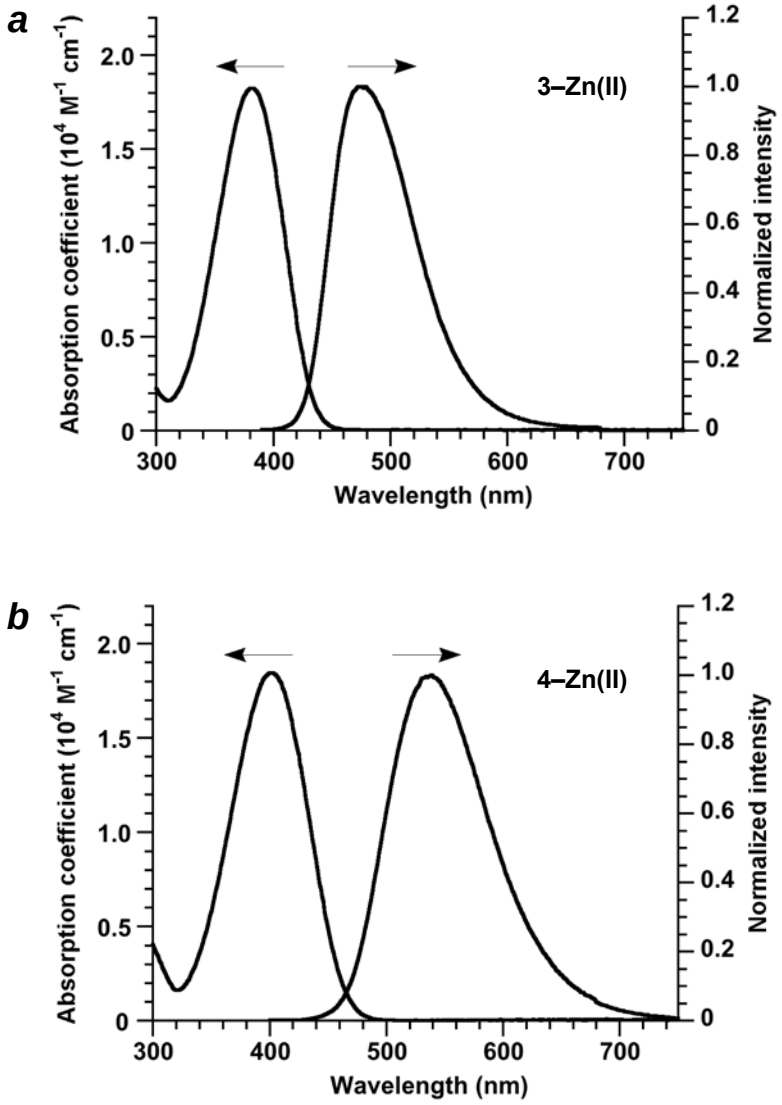

Figure S17. Optical absorption and normalized PL spectra of **3–Zn(II)** and **4–Zn(II)** in CH_3CN. Spectra recorded at 30 μM and 20 °C.

4. ^{1}H and ^{13}C NMR spectra

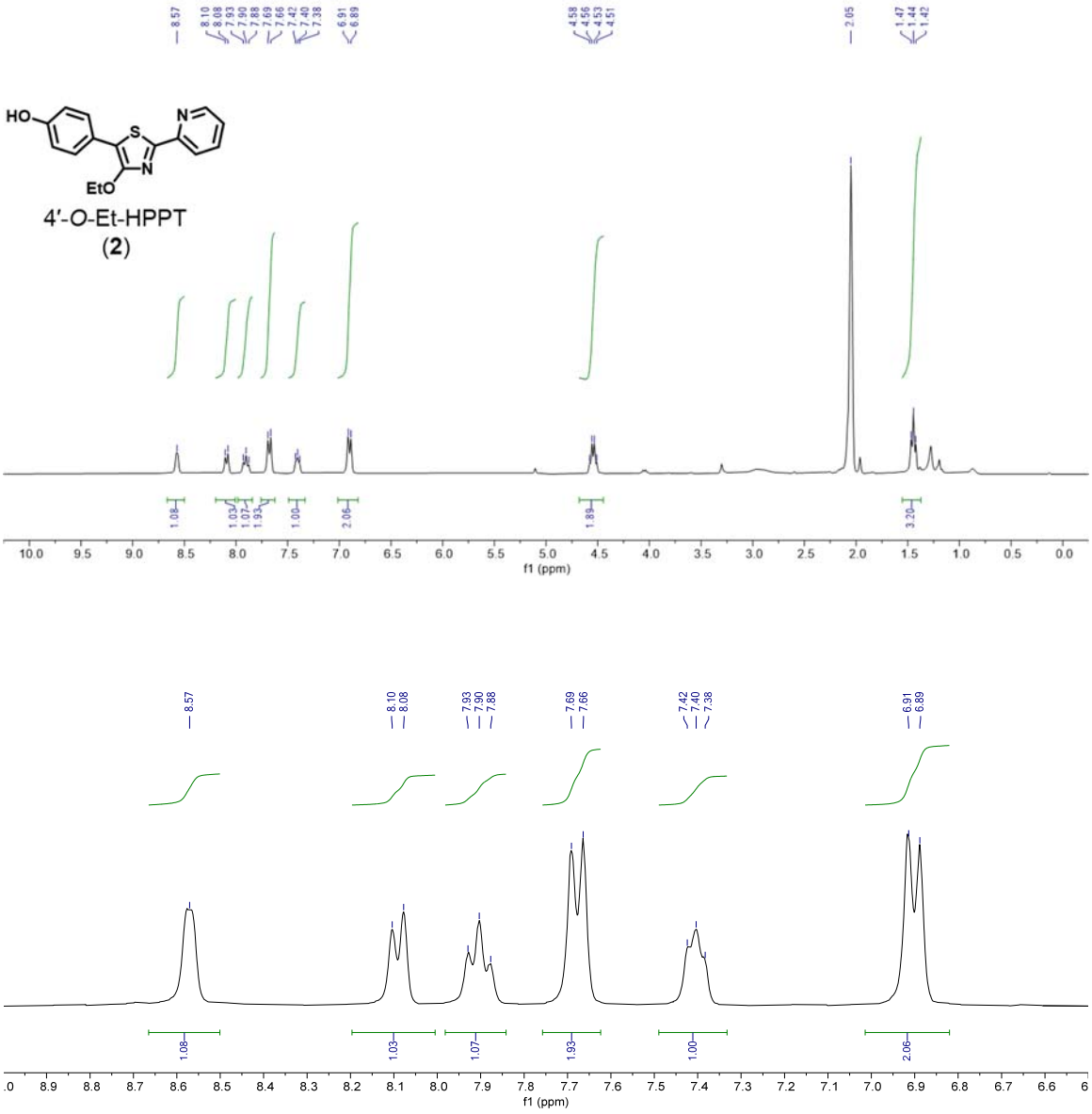

Figure S18. ^{1}H NMR spectra of **2** (300 MHz, acetone-d_6, 25 °C).

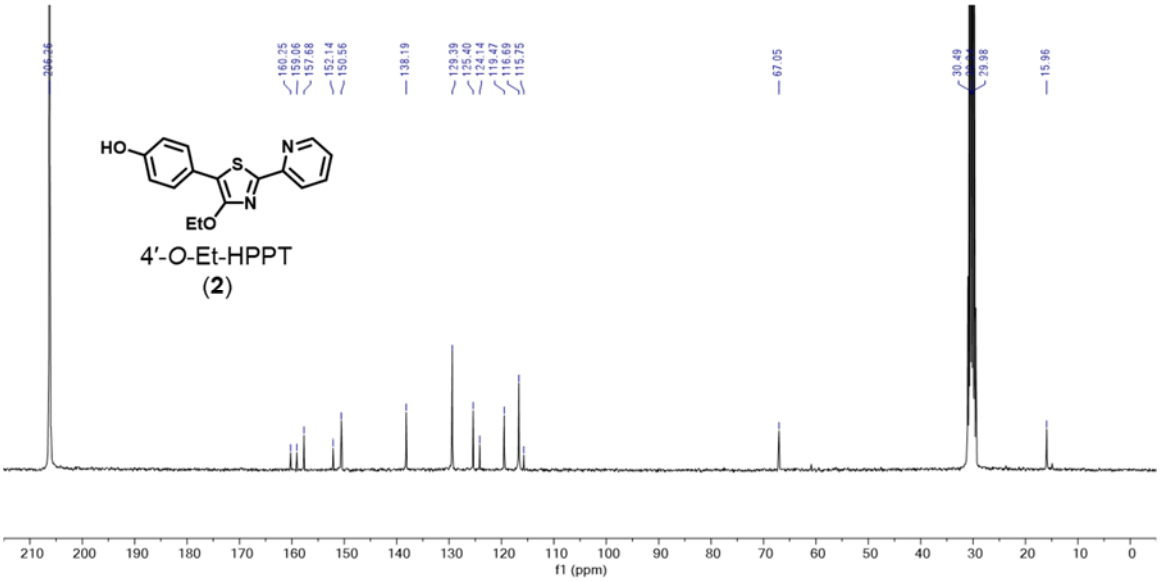

Figure S19. ^{13}C NMR spectrum of **2** (75 MHz, acetone-d_6, 25 °C).

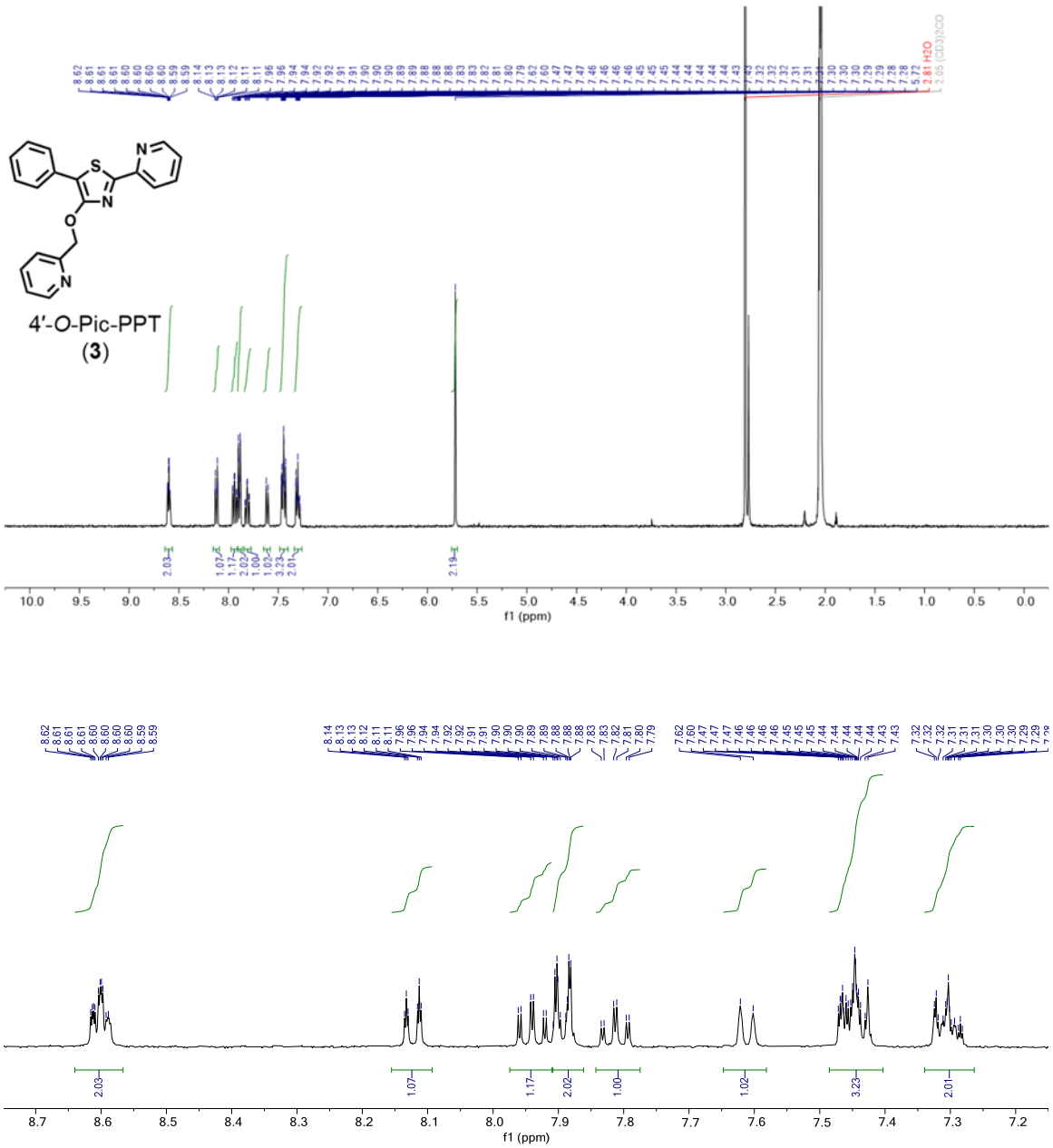

Figure S20. ^{1}H NMR spectra of **3** (400 MHz, acetone-d_6, 25 °C).

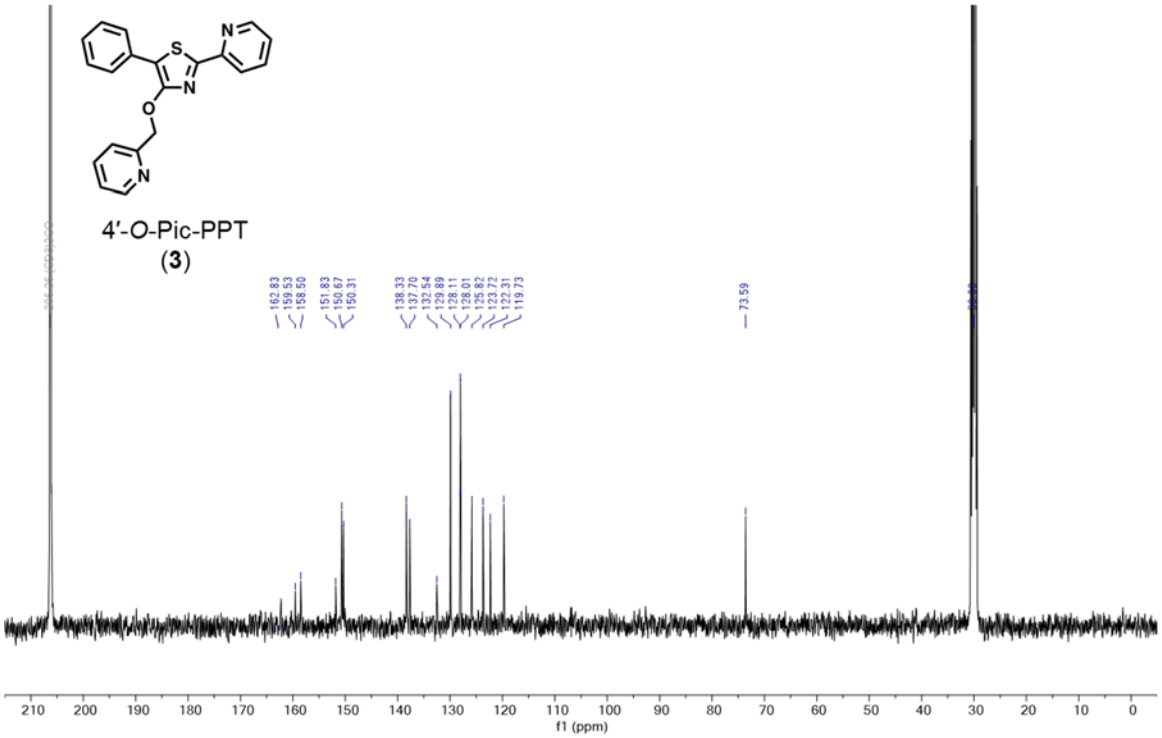

Figure S21. ^{13}C NMR spectrum of **3** (101 MHz, acetone-d_6, 25 °C).

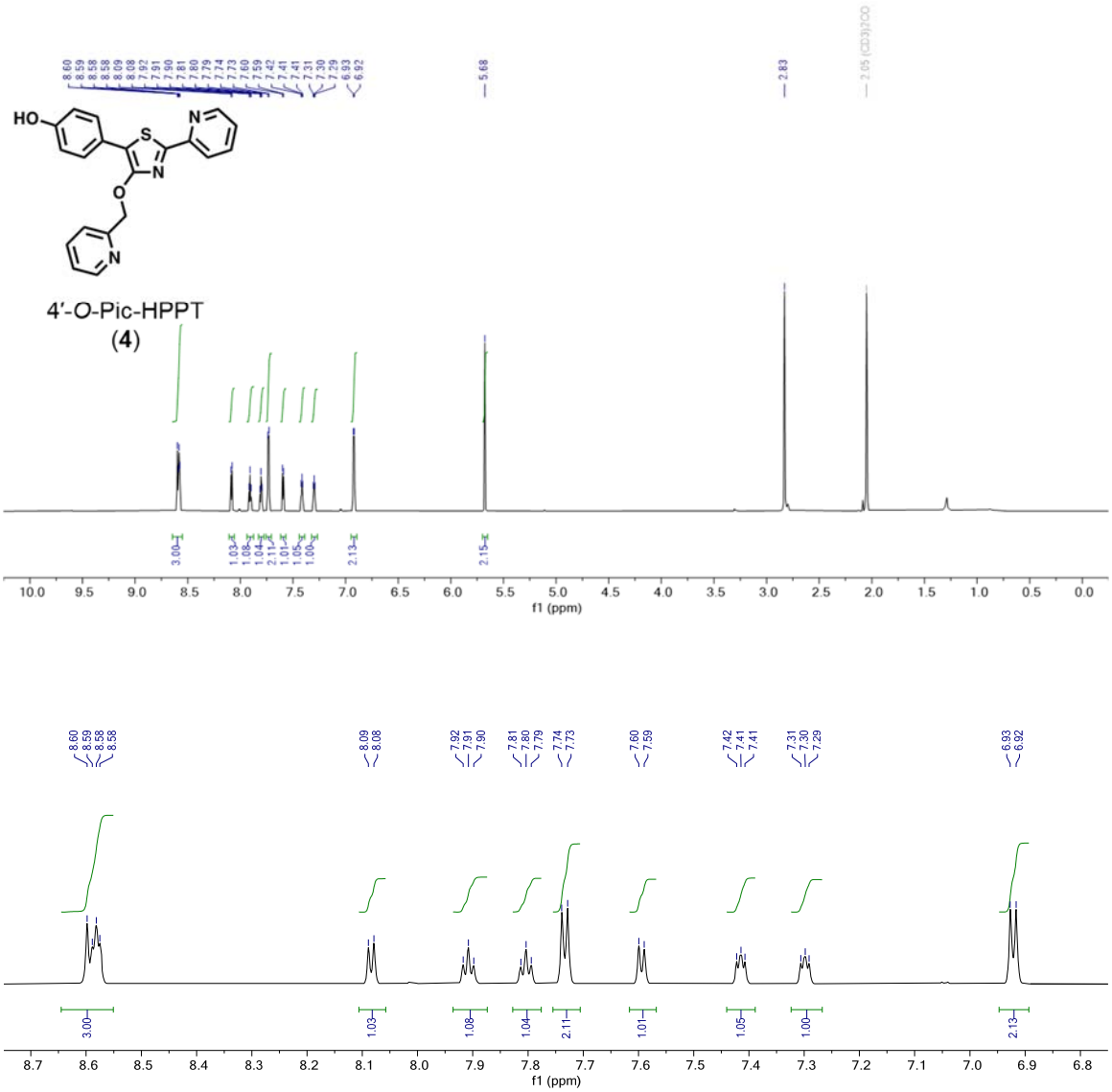

Figure S22. ^{1}H NMR spectra of **4** (800 MHz, acetone-*d*$_6$, 25 °C).

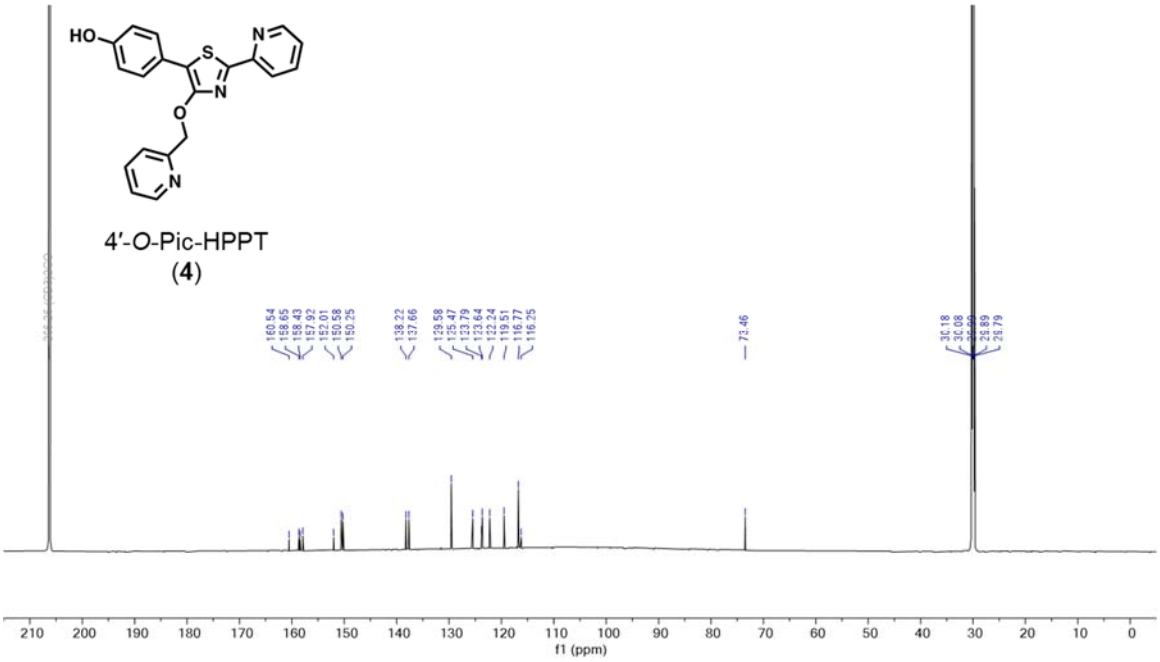

Figure S23. ^{13}C NMR spectrum of **4** (201 MHz, acetone-d_6, 25 °C).

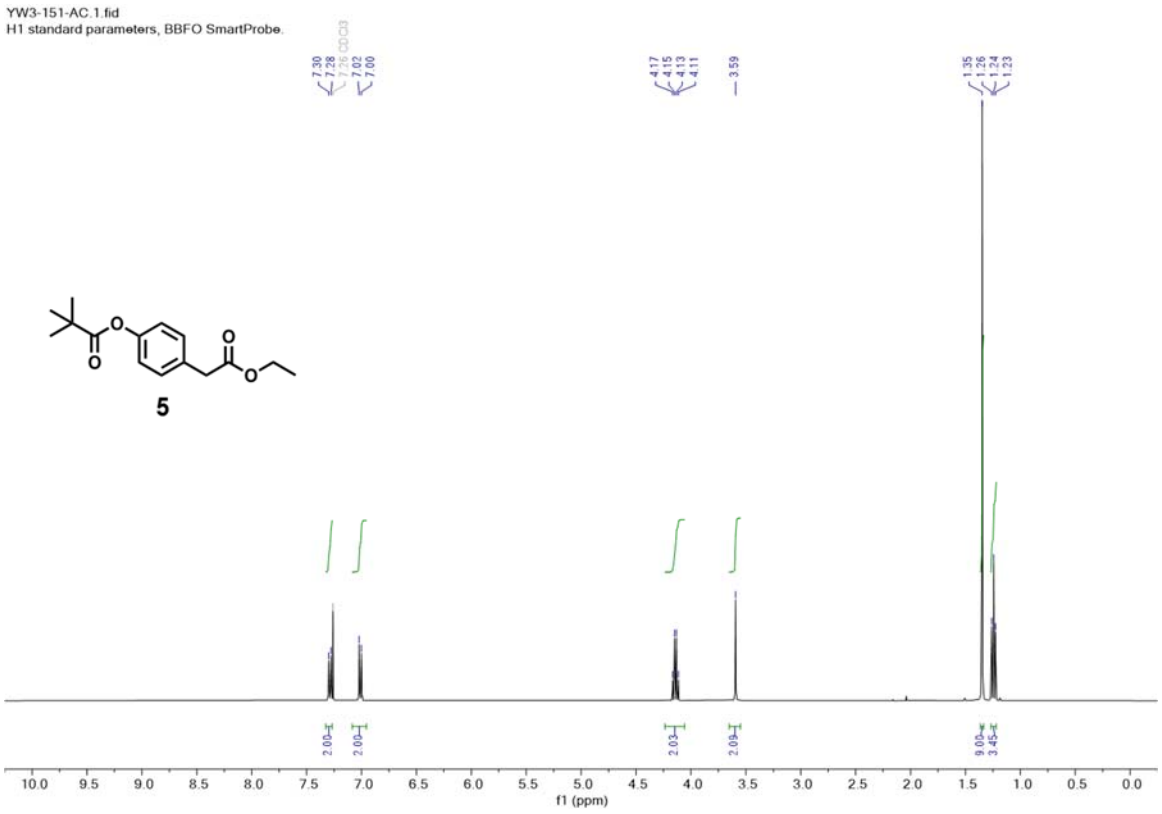

Figure S24. ^{1}H NMR spectra of **5** (400 MHz, $CDCl_3$, 25 °C).

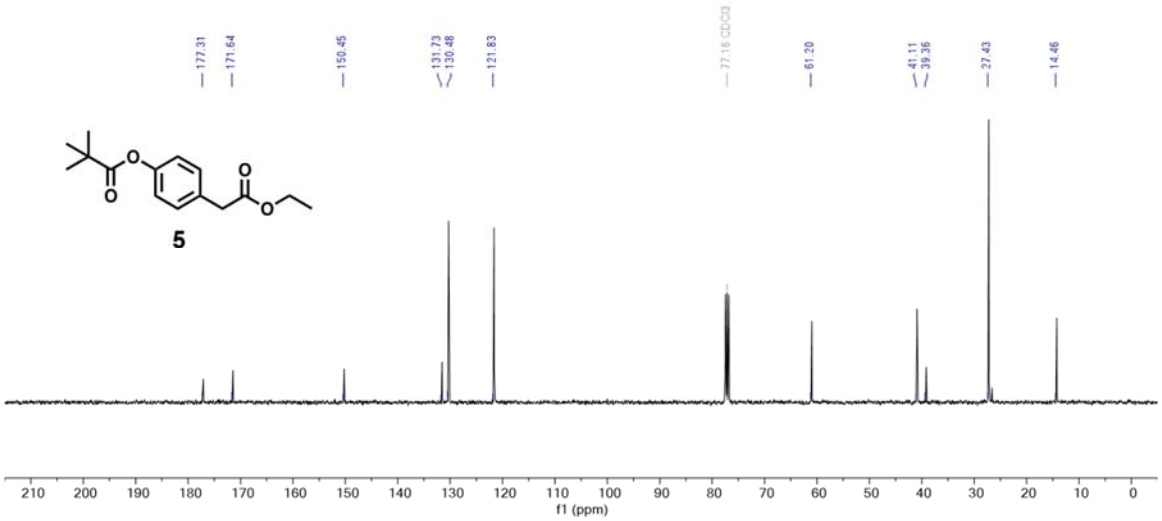

Figure S25. ^{13}C NMR spectrum of **5** (101 MHz, $CDCl_3$, 25 °C).

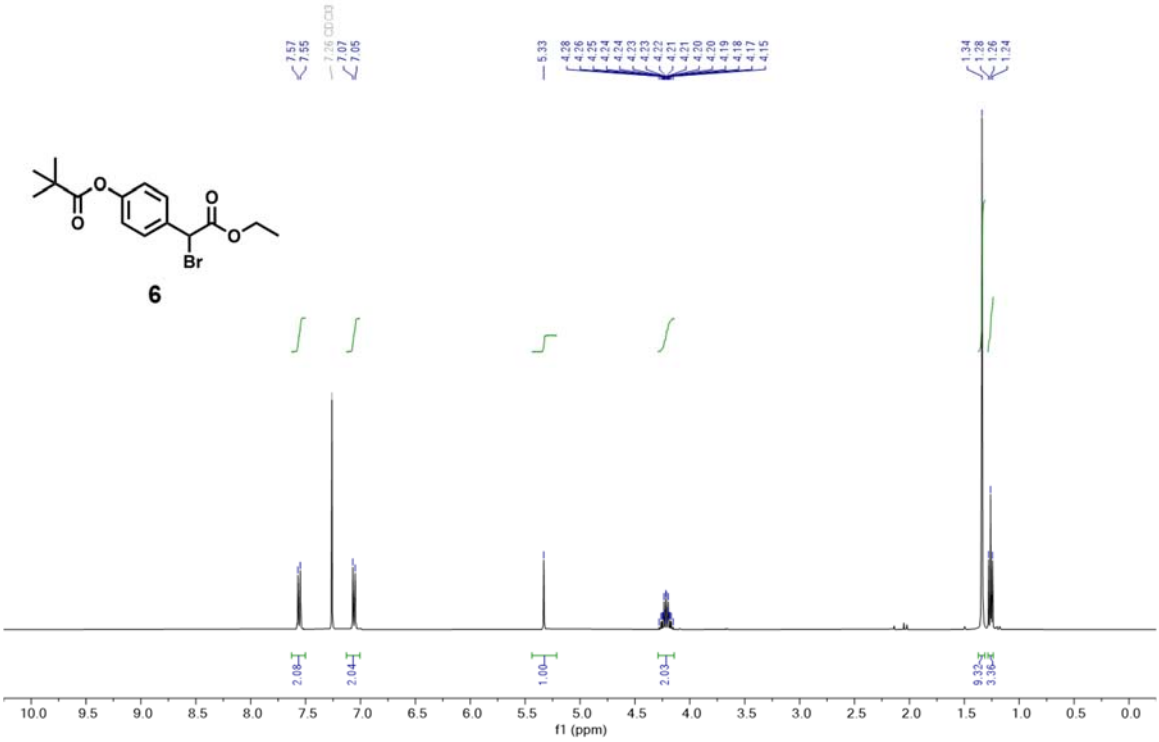

Figure S26. ^{1}H NMR spectra of **6** (400 MHz, $CDCl_3$, 25 °C).

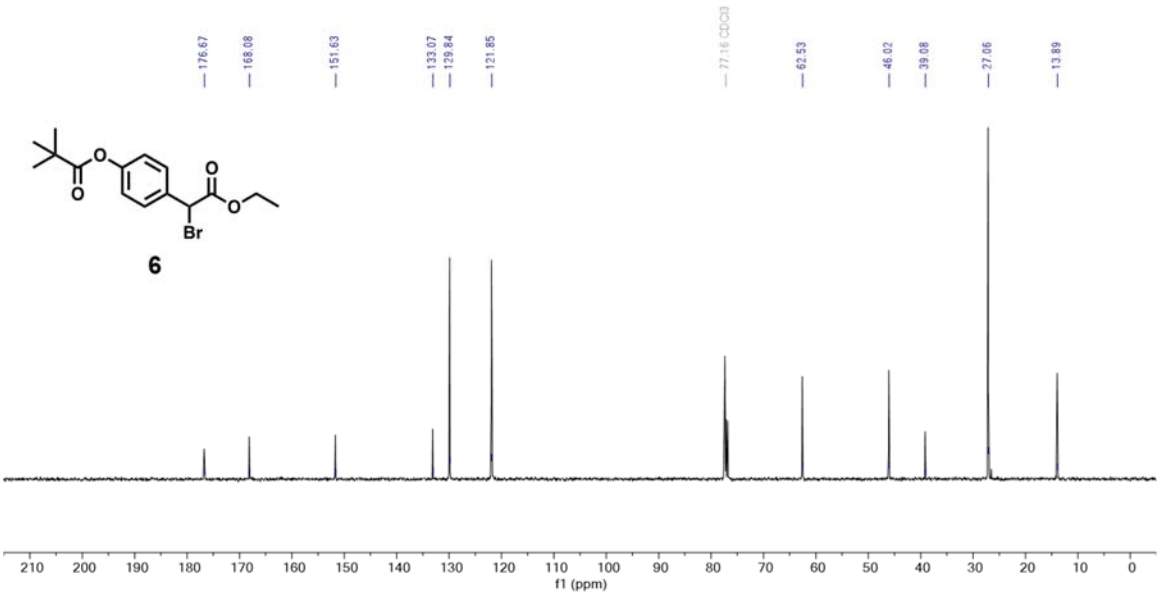

Figure S27. ^{13}C NMR spectrum of **6** (101 MHz, $CDCl_3$, 25 °C).

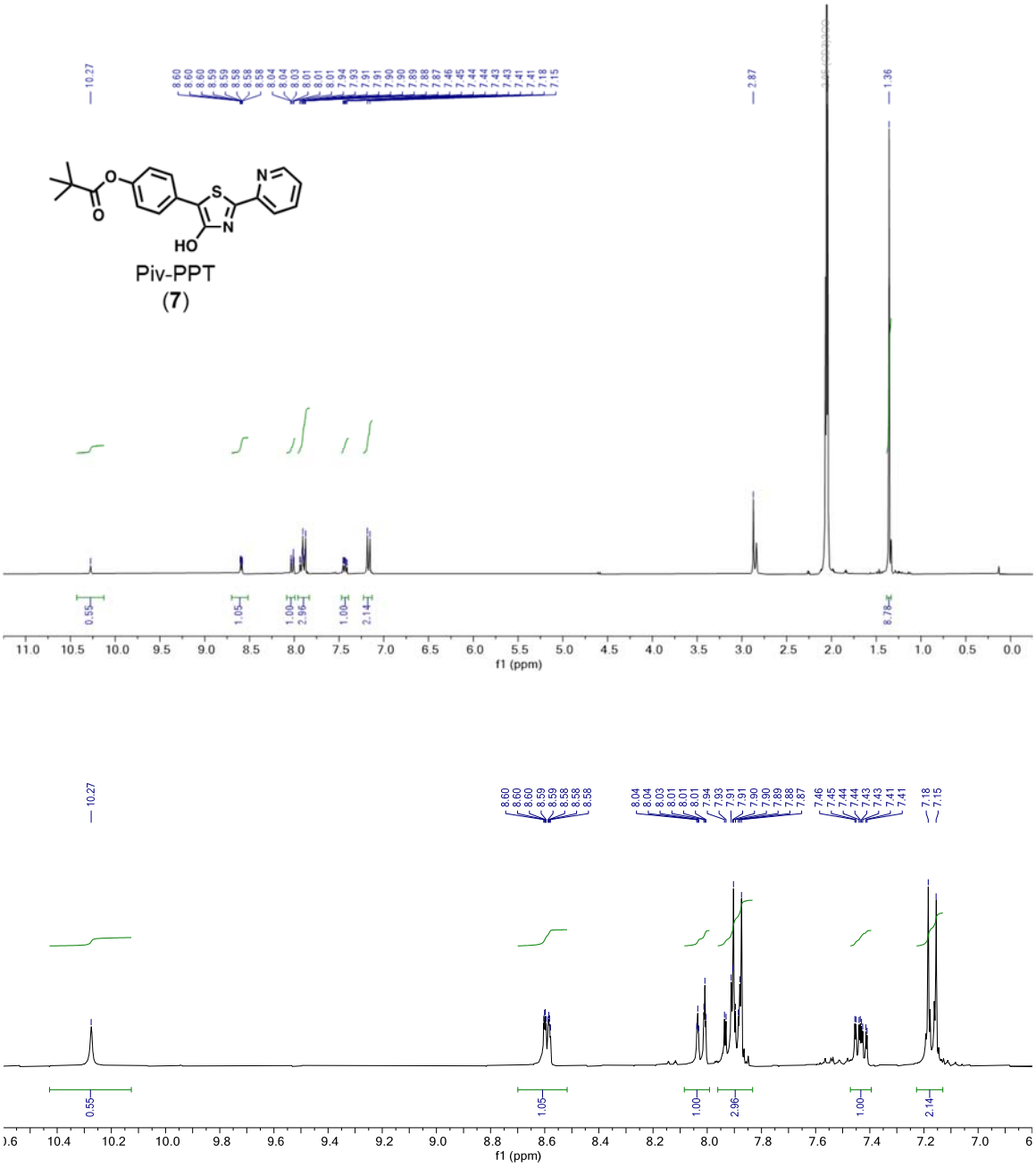

Figure S28. ^{1}H NMR spectra of **7** (300 MHz, acetone-*d*$_6$, 25 °C).

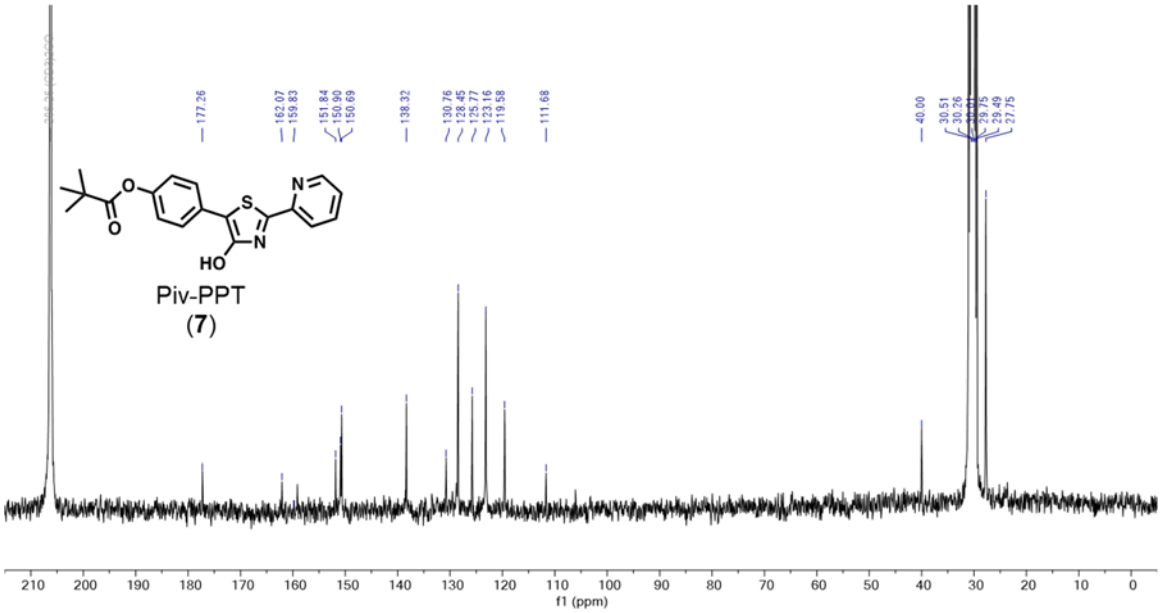

Figure S29. ^{13}C NMR spectrum of **7** (75 MHz, acetone-d_6, 25 °C).

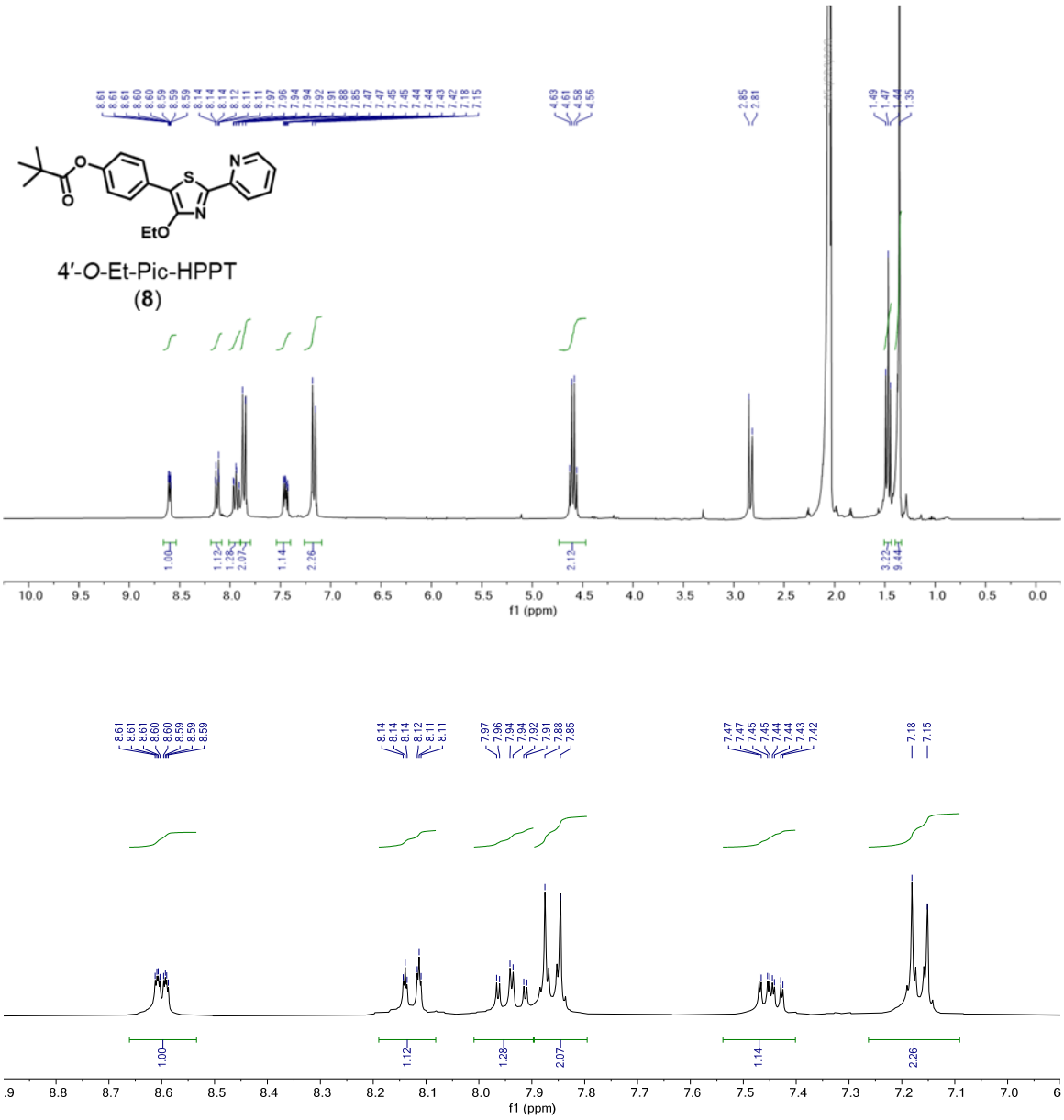

Figure S30. ^{1}H NMR spectra of **8** (300 MHz, acetone-d_6, 25 °C).

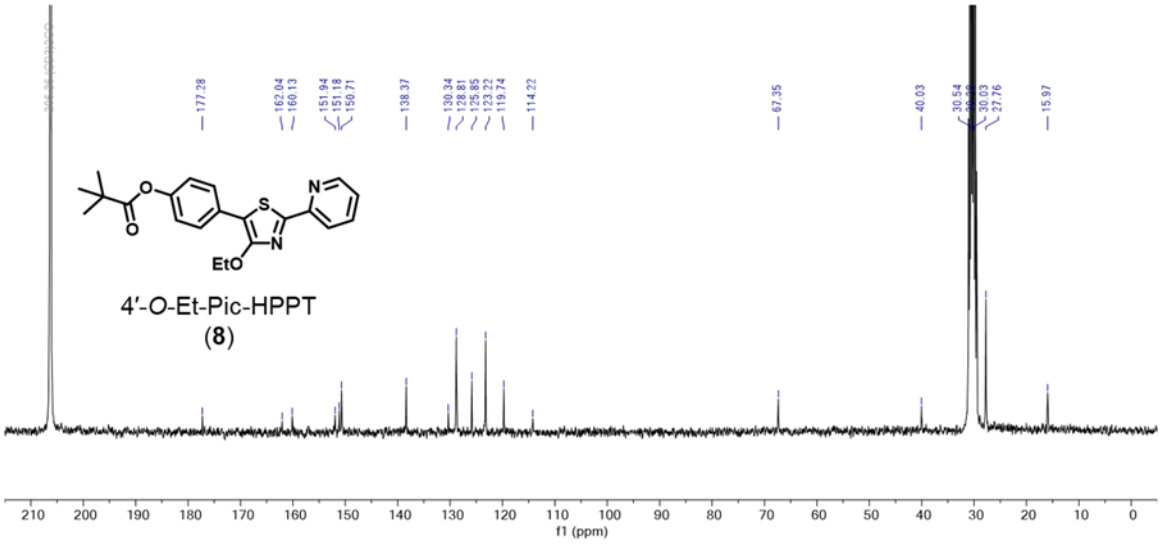

Figure S31. ^{13}C NMR spectrum of **8** (75 MHz, acetone-d_6, 25 °C).

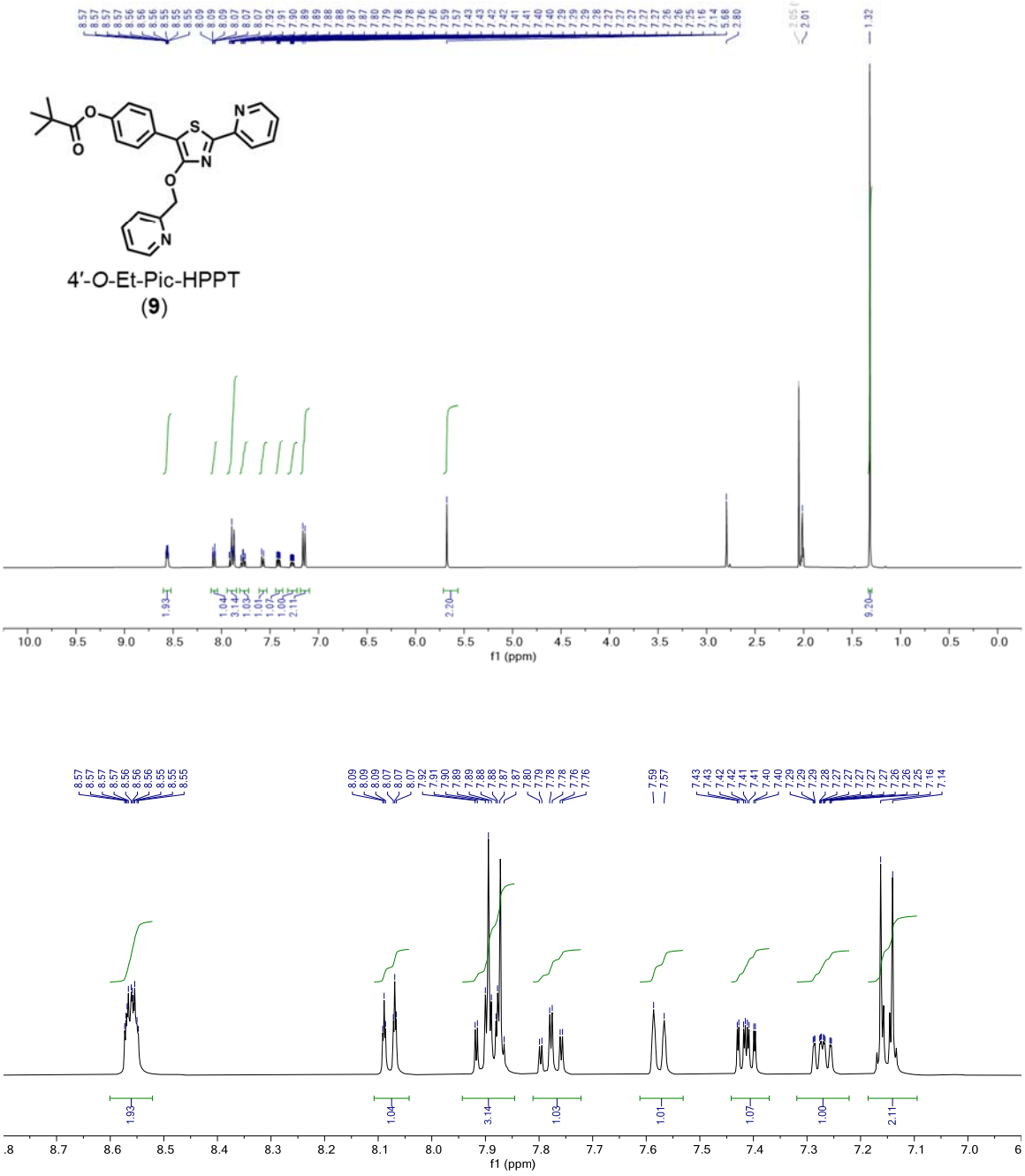

Figure S32. ^{1}H NMR spectra of **9** (400 MHz, acetone-d_6, 25 °C).

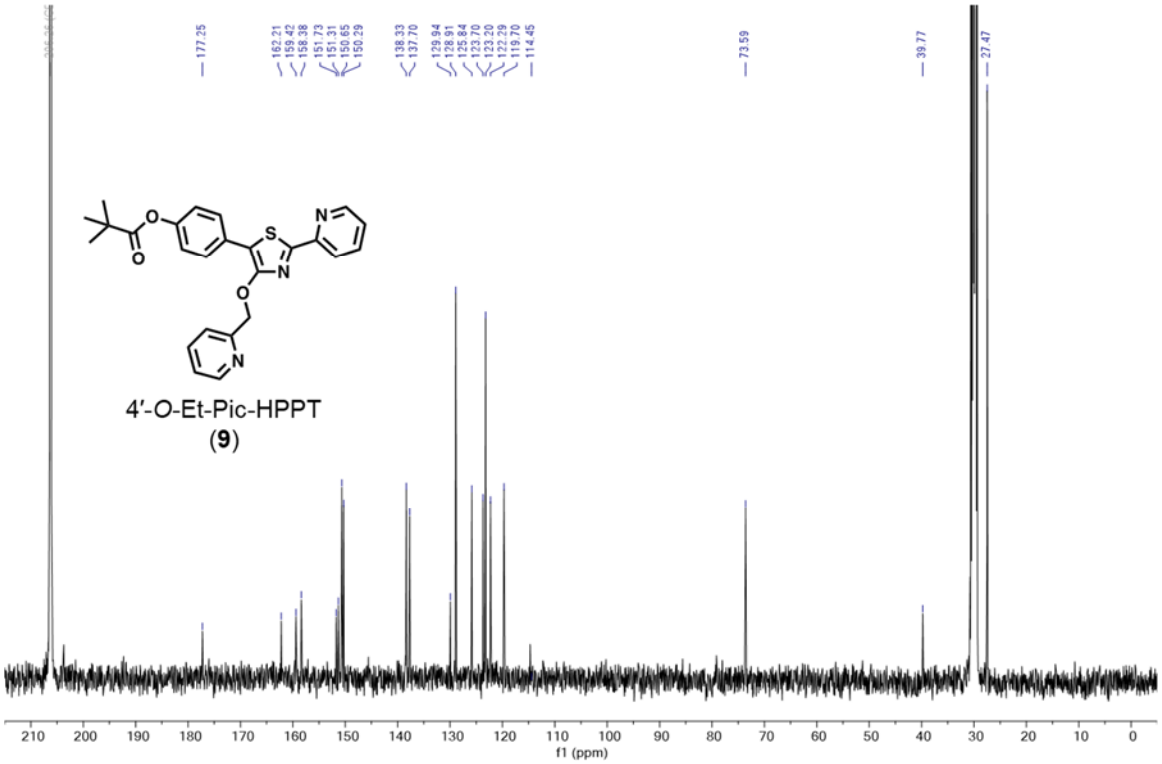

Figure S33. ^{13}C NMR spectrum of **9** (101 MHz, acetone-d_6, 25 °C).

6. References

1. (a) M. Kaufmann, M. L. Hupfer, T. Sachse, F. Herrmann-Westendorf, D. Weiß, B. Dietzek, R. Beckert, M. Presselt, Introducing double polar heads to highly fluorescent Thiazoles: Influence on supramolecular structures and photonic properties. *J. Colloid Interface Sci*., 2018, **526**, 410; (b) E. Täuscher, D. Weiß, R. Beckert, H. Görls, Synthesis and Characterization of New 4-Hydroxy-1,3-thiazoles. *Synthesis*, 2010, **10**, 1603; (c) S. Wolfram, H. Würfel, S. H. Habenicht, C. Lembke, P. Richter, E. Birckner, R. Beckert, G. Pohnert, A small azide-modified thiazole-based reporter molecule for fluorescence and mass spectrometric detection. *Beilstein J. Org. Chem*., 2014, **10**, 2470.
2. Apex 3 v2018.1-0, Saint V8.38A, SAINT V8.38A, (Bruker AXS, Inc., 2018).
3. G. M. Sheldrick, *Acta Cryst. A* 2008, **64**, 112.
4. G. M. Sheldrick, *Acta Cryst. C* 2015, **71**, 3.
5. G. M. Sheldrick, SHELXL2018.
6. C. B. Hübschle, G. M. Sheldrick, B. Dittrich, *J. Appl. Cryst*. 2011, **44**, 1281.
7. L. Krause, R. Herbst-Irmer, G.M. Sheldrick, D. Stalke *J. Appl. Cryst*. 2015, **48**, 3.
8. (a) H. A. Benesi, J. H. Hildebrand, A Spectrophotometric Investigation of the Interaction of Iodine with Aromatic Hydrocarbons *J. Am. Chem. Soc.*, 1949, **71**, 2703; (b) E. V. Anslyn, D. A.,Dougherty, *Modern Physical Organic Chemistry,* University Science Books, 2006, Ch. 4.